

A stellar census in globular clusters with MUSE: A spectral catalogue of emission-line sources

Fabian Göttgens¹, Tim-Oliver Husser¹, Sebastian Kamann², Stefan Dreizler¹, Benjamin Giesers¹, Wolfram Kollatschny¹, Peter M. Weilbacher³, Martin M. Roth³, and Martin Wendt⁴

¹ Institut für Astrophysik, Georg-August-Universität Göttingen, Friedrich-Hund-Platz 1, 37077 Göttingen, Germany
e-mail: fabian.goettgens@uni-goettingen.de

² Astrophysics Research Institute, Liverpool John Moores University, 146 Brownlow Hill, Liverpool L3 5RF, United Kingdom

³ Leibniz-Institut für Astrophysik Potsdam (AIP), An der Sternwarte 16, 14482 Potsdam, Germany

⁴ Institut für Physik und Astronomie, Universität Potsdam, Karl-Liebknecht-Str. 24/25, 14476 Golm, Germany

Received XXX; accepted YYY

ABSTRACT

Aims. Globular clusters produce many exotic stars due to a much higher frequency of dynamical interactions in their dense stellar environments. Some of these objects were observed together with several hundred thousands other stars in our MUSE survey of 26 Galactic globular clusters. Assuming that at least a few exotic stars have exotic spectra, that means spectra that contain emission lines, we can use this large spectroscopic data set of over a million stellar spectra as a blind survey to detect stellar exotica in globular clusters.

Methods. To detect emission lines in each spectrum, we model the expected shape of an emission line as a Gaussian curve. This template is used for matched filtering on the differences between each observed 1D spectrum and its fitted spectral model. The spectra with the most significant detections of H α emission are checked visually and cross-matched with published catalogues.

Results. We find 156 stars with H α emission, including several known cataclysmic variables (CV) and two new CVs, pulsating variable stars, eclipsing binary stars, the optical counterpart of a known black hole, several probable sub-subgiants and red stragglers, and 21 background emission-line galaxies. We find possible optical counterparts to 39 X-ray sources, as we detect H α emission in several spectra of stars that are close to known positions of Chandra X-ray sources. This spectral catalogue can be used to supplement existing or future X-ray or radio observations with spectra of potential optical counterparts to classify the sources.

Key words. globular clusters: general – Stars: emission-line, Be – novae, cataclysmic variables – catalogs – techniques: imaging spectroscopy

1. Introduction

In the dense stellar environments of globular clusters (GCs), the frequent interactions between stars produce a wealth of stellar exotica. This includes interacting binary systems and end states of stellar evolution, such as cataclysmic variables (CVs, Ivanova et al. 2006), pulsars (Ransom 2007), and planetary nebulae (PNe) (Jacoby et al. 2017). Emission lines are expected to appear in the optical spectra in at least some of these stellar types; those stars are then classified as emission-line stars. Because of the old age of globular clusters and their stars, some types of emission-line stars still present in the Milky Way disc do not exist (anymore) in globular clusters, for example Wolf-Rayet stars or Be stars.

In recent years, several stellar-mass BH candidates have been found in binary systems in globular clusters (Strader et al. 2012; Giesers et al. 2018). Photometric observations suggest that some of these systems could be H α emitters. While stellar-mass BHs were long thought to be ejected from GCs during cluster evolution, the discoveries of stellar-mass BH candidates in multiple clusters indicate a large population of these black holes inside evolved GCs (Strader et al. 2012; Askar et al. 2018; Kremer et al. 2018).

CVs are binary systems consisting of a hot, compact white dwarf and a dwarf star in a close orbit. The white dwarf accretes

material from its companion star that accumulates in an accretion disc. In the dense stellar environments of globular clusters, CVs and progenitor systems are influenced by dynamical interactions, with up to 50 % forming via a binary encounter (Ivanova et al. 2006, but also see Belloni et al. 2019). The number of predicted CVs per cluster is on the order of 200, but the number of observed CV candidates or confirmed CVs in the literature is much lower (Knigge 2012). CV candidates can be found with photometric observations, for example looking for dwarf nova outbursts, for stars with UV excess (e.g. Sandoval et al. 2018), for outliers in the colour-magnitude diagram of a GC (e.g. Campos et al. 2018), or using H α surveys (Knigge 2012). Alternatives for detecting CVs are far-ultraviolet spectroscopy which has also been useful for detecting CVs in globular clusters (Knigge et al. 2003), and X-ray observations. Follow-up optical spectroscopy to confirm CVs in GCs is difficult because of the crowded fields and the intrinsically low brightness of CVs.

When a nova occurs in a CV, it can leave behind a visible emission nebula as a remnant such as the one in NGC 6656 (Göttgens et al. 2019). Nova remnants are not the only type of nebula in GCs, another type are planetary nebulae of which four are known in the Galactic GC system. Even this low number of PNe in GCs is too high because the low masses of AGB stars should prohibit the formation of PNe (Jacoby et al. 1997). This lead to the prediction that PNe in GCs are formed by a different

mechanism, possibly by binary interaction (Jacoby et al. 1997, 2017).

Many stellar exotica in GCs have been found using X-ray observations. However, it is less clear which optical counterpart belongs to an X-ray source when only broad-band photometry is available. In this case, a counterpart is identified if it is an outlier in the optical CMD with respect to all other cluster stars, that is if its separation from the main sequence or the red-giant branch is too large, or if its color is too blue (e. g. Bassa et al. 2004; Webb et al. 2004). Similarly, the an optical emission lines in a spectrum of a star close to an X-ray source could also indicate it is a counterpart.

Previous optical surveys for typical classes of emission-line objects used photometric observations and the on/off-band technique, variability, or anomalous colours to detect candidate objects: Jacoby et al. (1997) conducted the most successful PNe survey for GCs, Knigge (2012) lists several CV surveys. Spectroscopic follow-up observations are then used to confirm the classification and to derive more properties of the source.

The data used in this paper were obtained with MUSE (Bacon et al. 2010), a panoramic integral-field spectrograph at the Very Large Telescope, as part of a survey of Galactic globular clusters. With the MUSE data already obtained, emission-line objects can be found without the need of additional observations because both spatial and spectral information is present. While Roth et al. (2018) demonstrated the efficiency of MUSE at detecting emission-line objects including Wolf-Rayet stars, supernova remnants, H II regions, and PNe in the galaxy NGC 300, we can for the first time conduct a blind survey for emission-line stars in Galactic globular clusters.

2. Data

2.1. Observations and reduction

This work makes use of all data taken with MUSE for our survey of 26 Galactic globular clusters between September 2014 and March 2019 (PI: S. Dreizler, S. Kamann).¹ MUSE has a large field of view ($1' \times 1'$) combined with a spatial sampling of $0.2''$ and an intermediate resolution R between 1800 and 3500 in the spectral range from 4750 to 9350 Å. The observations and the analysis steps have been described in detail by Kamann et al. (2018) and are summarised here. In contrast to Kamann et al. (2018), this work also includes data from observations made after October 2016. Table 1 gives an overview of the observation statistics for each cluster.

Each observation was reduced with the standard MUSE pipeline (Weilbacher et al. 2012, 2014) which calibrates the images from the 24 MUSE spectrographs, including cosmic ray rejection, and transforms them into a datacube. In the next step, single stellar spectra are extracted with a point-spread-function (PSF) from this datacube. The extractions use the PSF-fitting developed in Kamann et al. (2013) to measure the PSF parameters and determine stellar positions in the datacube as a function of wavelength. We mostly use stellar positions from the ACS survey of Galactic globular clusters (Sarajedini et al. 2007; Anderson et al. 2008, hereafter ACS catalogue) as an input for the extraction, see Table 2 in Kamann et al. (2018) for details. The extracted spectra are then analysed with respect to the Göttingen spectral library (Husser et al. 2013), a grid of synthetic spectral

Table 1. Overview of globular cluster data used in this paper. This includes all observations made between September 2014 and March 2019.

NGC (1)	Name (2)	$N_{\text{pointings}}$ (3)	N_{epochs} (4)	ToT [h] (5)	N_{spectra} (6)	N_{stars} (7)
104	47 Tuc	10	13	12.2	309911	32055
362		6	2	1.3	24049	9363
1851		4	6.5	4.7	67267	11614
1904	M 79	4	5.5	2.5	32597	5669
2808		4	2	1.2	20230	8040
3201		5	12	11.6	61855	4503
5139	ω Cen	10	10.5	12.2	335614	45616
5286		1	4	1.0	17954	8282
5904	M 5	6	2	2.3	51450	18203
6093	M 80	4	2	1.6	21051	9153
6121	M 4	2	1	0.1	1251	1067
6218		4	3	3.0	22989	6616
6254	M 10	8	1.5	3.3	29633	14296
6266	M 62	4	3	2.0	39190	15900
6293		1	2	0.1	2154	1326
6388		4	4	2.2	46600	14484
6441		4	4	2.8	43473	13247
6522		1	3	0.2	7564	3567
6541		5	2	1.9	35352	12003
6624		1	2	0.5	8300	4556
6656	M 22	4	2.5	2.2	36609	13204
6681	M 70	1	2	0.8	8283	4773
6752		8	2	3.0	31070	14086
7078	M 15	4	3	1.6	40606	18015
7089	M 2	4	4	2.4	47764	15309
7099	M 30	4	3.5	2.6	34176	9111
total		114	103.0	80.8	1379362	316428

Notes. (1) NGC number. (2) Alternative identifier (if any). (3) Number of pointings. This number roughly corresponds to the covered field of view in arcminutes. (4) Average number of epochs available for each pointing. (5) Total integration time in hours. (6) Number of extracted spectra. (7) Number of stars with at least one extracted spectrum.

models suitable for most stars in globular clusters. A chi-square fit on the full spectrum minimises the difference between the observed spectrum and a model spectrum by interpolating between grid spectra to determine the stellar parameters effective temperature, metallicity, and the radial velocity (Husser et al. 2016).

In addition to the spectra obtained from single observations, we also use these to create a high-signal-to-noise spectrum for each star. We shift all spectra of each star to the Sun's restframe and add the flux weighted by the signal-to-noise ratio of the spectrum. These combined spectra are then analysed in a similar way to the one described above.

2.2. Residuals from spectral fitting

The residuals from the spectral fitting are defined as the difference between model and observation. We can use these residuals to detect emission-line stars because the spectral library does not contain spectra with emission lines, in other words if an emission line is present in the observed spectrum, it will also be visible in the residuals.

The residuals can contain random noise, additional absorption from the interstellar medium (Wendt et al. 2017), systematic errors of the model spectra (e.g. absorption lines that only exist in the models, see Fig. 1, or vice versa), instrumental systemat-

¹ ESO Program IDs: 094.D-0142, 095.D-0629, 096.D-0175, 097.D-0295, 098.D-0148, 099.D-0019, 0100.D-0161, 0101.D-0268, and 0102.D-0270.

ics, and true emission lines. If the fit did not find the global minimum of the chi-square space, the residuals will contain a large amount of stellar light. In this case, the parameters determined by the fit do not necessarily describe the star, and the residuals can cause false positive detections of emission lines.

It is also possible that the spectral model grid does not contain a suitable model for the observed spectrum. This occurs for horizontal branch stars and some M stars. Spectra of M stars contain strong molecular bands which have a great influence on the overall spectral appearance. A slight mismatch in the fit of an M star spectrum has a large impact on the residuals. If a spectrum of an M star contains emission lines, the effect of the emission lines on the residuals could be smaller than the effects of spectrum mismatch. In these cases, the method based on matched filtering to detect emission lines described in Sect. 3.1 is not reliable and the detection fails. However, the method based on the residuals without convolution (Sect. 3.2) still works in these cases.

3. Emission line detection

As shown in Table 1, we extract millions of stellar spectra from our observations. The large number of observed spectra makes it impossible to visually check each of them.

We use two approaches to detect emission lines in the residuals from the spectral fit. The first approach based on matched filtering is widely applied to similar problems, for example in gravitational-wave detection (Abbott et al. 2016) and to detect emission-line galaxies in MUSE datacubes (Herenz & Wisotzki 2017). The second method uses only the residuals and a running estimate of the noise. This method is used as a backup whenever matched filtering fails to detect a signal, because it is much simpler and more robust but also produces more false detections. Both approaches assign a significance to each detection which is then used to select the most promising candidates for visual inspection.

We stress that we do not use existing catalogues of emission-line stars as a prior to find those in our data. Since the aim of this work is to find new and unexpected sources, we use external catalogues only after our methods identify a possible spectrum with emission lines.

3.1. Matched filtering with mean absolute deviation

Because of the large dataset, we need to choose an approach that is fast and can extract potentially weak signals. One algorithm with these properties is called *matched filtering* (see Vio & Andreani 2016, and references therein) that requires prior knowledge about the expected signal. We assume that each emission line can be described by a Gaussian curve with a standard deviation (width) of 5 Å. This width is determined from simulations in Sect. 3.3. Instead of applying matched filtering directly on the observed spectral flux (top panel in Fig. 1), we use it on the residuals that result from spectral fitting (see bottom panel of Fig. 1). Mathematically, matched filtering computes the convolution $C(\lambda)$ of the filter (the expected line profile) and the residual flux. As shown in the bottom panel in Fig. 1 (dashed line), the convolution is high at a certain wavelength when the expected flux shape matches the measured flux. On the other hand, noise – which is typically only a few pixels wide – is smoothed out, that means the convolution gives a much lower value as it would for real emission. Compared to the convolution of noise or continuum flux with a Gaussian, emission flux appears in the convolution as a peak centred at the emission line. We detect an

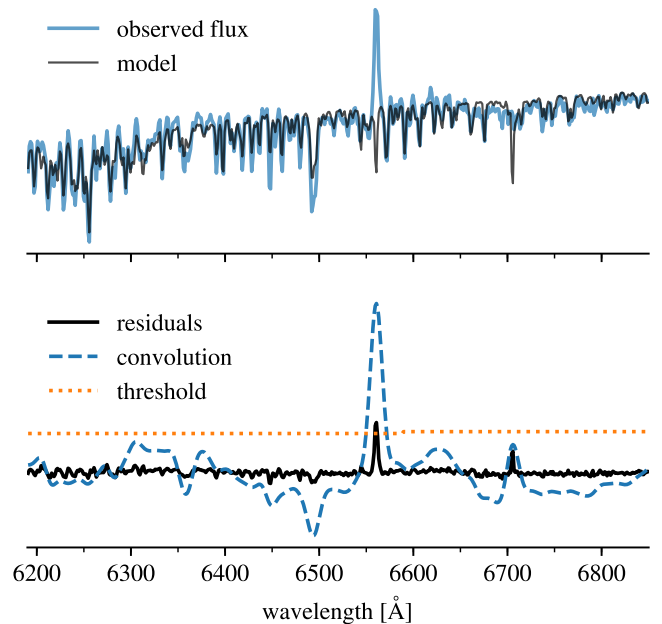


Fig. 1. Illustration of emission-line detection with matched filtering. Top: observed flux of V190 in NGC 6266 with H α emission and the fitted spectral model. Bottom: The H α emission line is still present in the residuals, as well as an absorption line at 6700 Å which is only found in the models. The convolution with a Gaussian increases the emission line above the threshold calculated from the mean absolute deviation of the residuals.

emission signal at wavelength λ_e if the convolution at that point is larger than some threshold function $t(\lambda)$ at the same point. The threshold function is constructed as the median absolute deviation (MAD) calculated separately for wavelength bins of the residual flux (dotted line in the bottom panel of Fig. 1). By construction, the ratio $D_s = C(\lambda_e)/t(\lambda_e)$ is higher for more prominent emission signals. We call this ratio detection significance and use it to select promising candidates for visual inspection by requiring that a detection lies above a minimum value of D_s . The detection efficiency depends on this choice and it is analysed with simulated emission lines in Sect. 3.3.

3.2. Plain residuals and running noise estimate

This section presents a more robust method of detecting emission lines that relies on fewer assumptions. Similar to the method based on matched filtering, it relies on the residuals from the spectral fit. The residual flux $r_i = r(\lambda_i)$ at each wavelength point λ_i is compared to the residual noise s_i at the adjacent wavelengths. We locally estimate the noise from the difference of the ninetyth and tenth percentile of the residual flux in a 100 Å window centred at λ_i . Since the spectral model does not describe the observed flux perfectly, the residuals contain noise and systematic effects (see Sect. 2.2). We account for these outliers in the residual flux by using percentiles instead of extrema or measures that are sensitive to outliers. At each wavelength, the ratio of residual flux to the noise estimate $D_s = r_i/s_i$ represents the significance of an emission-line detection. For comparison, if the noise was normally distributed with a variance σ^2 , a ratio of $D_s = 1$ corresponds to an observation with a significance of $\approx 1.3\sigma$.

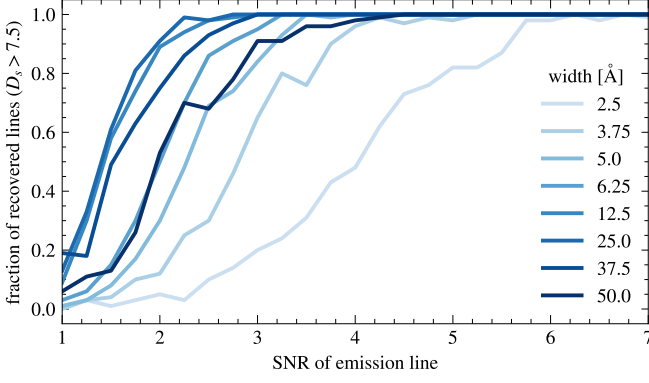


Fig. 2. Fraction of simulated emission lines that are recovered with a filter width of 6 Å depending on the simulated line width. Only detections above a detection significance $D_s > 7.5$ are taken into account.

Simulations show that this method works well for narrow emission lines but not for broad ones. This is because a broad emission line increases the residuals over a broader spectral range, and thus the percentiles used to estimate the noise increase as well. Since this increases s_i but not the amplitude r_i , the detection significance D_s decreases accordingly.

3.3. Detection efficiency

We estimate the fraction of emission signals recovered with the method based on matched filtering described in Sect. 3.1 with simulated emission lines. The detection significance of an emission-line candidate depends on the amplitude and width of the emission peak in the residual flux, and on the noise of the spectrum and the width of the Gaussian filter. We construct emission lines by sampling a Gaussian curve with a standard deviation σ that we vary between 3 and 60 Å, its amplitude is set to one. We draw noise from a normal distribution with a width of $(\text{SNR})^{-1}$ and add it to the signal. For each simulated emission line, we apply the detection method (Sect. 3.1) and calculate the detection significance for filter widths of 6, 25, 60, and 120 Å. We note that this leads to an estimate of how effective the detection methods is with respect to the amplitude of an emission line and not the total line flux.

The main results of this analysis are: We can find broad synthetic emission lines of several tens of Ångström even with a narrow filter width of 6 Å while the reverse is not true. As Fig. 2 shows, we recover about 50 % of broad emission lines (≈ 40 Å) with a filter width of 6 Å for a SNR of 2 if we only take detections with $D_s > 7.5$ into account. This fraction increases with increasing SNR and with decreasing emission-line width (except for very narrow widths < 5 Å below the filter width). We conclude from these simulated emission lines that for our data the choice of a 6 Å filter is reasonable, and $D_s > 7.5$ is a good lower limit for a detection to be inspected further. The filter width is four to five times the FWHM of the line-spread-function (LSF) of MUSE which varies between 2.5 and 3 Å depending on wavelength (Bacon et al. 2017). In principle, one could choose the threshold D_s much lower than this for the price of many more detections to inspect, which will contain a much higher frequency of false positives. The choice of $D_s > 7.5$ is also justified by the low empirical true positive rate of $\lesssim 5\%$ below this limit (see Sect. 4.1 and Fig. 4).

Table 2. Limiting fluxes for all clusters, calculated using a broad emission line (40 Å) and also valid for narrow lines (see text). Uncertainties give the central 80 % of the distribution on the main-sequence (MS), main-sequence turn-off (TO), and red giant branch (RGB).

Cluster	$\log_{10} F_{\min} [\text{erg/s/cm}^2/\text{Å}]$		
	MS	TO	RGB
NGC 104	$-16.9^{+0.3}_{-0.5}$	$-16.7^{+0.3}_{-0.5}$	$-16.3^{+0.4}_{-0.2}$
NGC 1851	$-17.5^{+0.3}_{-0.2}$	$-17.3^{+0.3}_{-0.3}$	$-17.0^{+0.5}_{-0.3}$
NGC 1904	$-17.5^{+0.3}_{-0.2}$	$-17.4^{+0.3}_{-0.2}$	$-16.9^{+0.4}_{-0.2}$
NGC 2808	$-17.4^{+0.3}_{-0.2}$	$-17.3^{+0.3}_{-0.2}$	$-16.8^{+0.4}_{-0.2}$
NGC 3201	$-17.6^{+0.3}_{-0.2}$	$-17.4^{+0.3}_{-0.1}$	$-16.6^{+0.1}_{-0.1}$
NGC 362	$-17.1^{+0.3}_{-0.2}$	$-17.1^{+0.3}_{-0.2}$	$-16.5^{+0.5}_{-0.3}$
NGC 5139	$-17.1^{+0.3}_{-0.2}$	$-16.9^{+0.3}_{-0.2}$	$-16.5^{+0.2}_{-0.2}$
NGC 5286	$-17.6^{+0.3}_{-0.2}$	$-17.5^{+0.3}_{-0.2}$	$-17.2^{+0.4}_{-0.2}$
NGC 5904	$-17.4^{+0.3}_{-0.3}$	$-17.2^{+0.3}_{-0.3}$	$-16.6^{+0.4}_{-0.1}$
NGC 6093	$-17.5^{+0.2}_{-0.2}$	$-17.5^{+0.3}_{-0.2}$	$-17.1^{+0.4}_{-0.3}$
NGC 6121	$-16.9^{+0.3}_{-0.1}$	$-16.9^{+0.2}_{-0.1}$	$-16.4^{+0.0}_{-0.0}$
NGC 6218	$-17.8^{+0.3}_{-0.1}$	$-17.4^{+0.2}_{-0.1}$	$-16.9^{+0.3}_{-0.1}$
NGC 6254	$-17.6^{+0.3}_{-0.3}$	$-17.4^{+0.3}_{-0.2}$	$-16.7^{+0.3}_{-0.1}$
NGC 6266	$-17.6^{+0.3}_{-0.2}$	$-17.4^{+0.4}_{-0.2}$	$-16.9^{+0.5}_{-0.2}$
NGC 6293	$-17.1^{+0.2}_{-0.2}$	$-17.2^{+0.2}_{-0.2}$	$-16.8^{+0.4}_{-0.2}$
NGC 6388	$-17.5^{+0.2}_{-0.2}$	$-17.4^{+0.3}_{-0.2}$	$-17.1^{+0.4}_{-0.2}$
NGC 6441	$-17.6^{+0.2}_{-0.1}$	$-17.5^{+0.3}_{-0.2}$	$-17.2^{+0.3}_{-0.2}$
NGC 6522	$-17.4^{+0.3}_{-0.1}$	$-17.4^{+0.3}_{-0.1}$	$-17.0^{+0.3}_{-0.2}$
NGC 6541	$-17.4^{+0.3}_{-0.2}$	$-17.3^{+0.3}_{-0.2}$	$-16.9^{+0.3}_{-0.1}$
NGC 6624	$-17.6^{+0.3}_{-0.2}$	$-17.6^{+0.3}_{-0.2}$	$-17.2^{+0.5}_{-0.2}$
NGC 6656	$-17.2^{+0.3}_{-0.3}$	$-17.1^{+0.4}_{-0.3}$	$-16.5^{+0.3}_{-0.1}$
NGC 6681	$-17.8^{+0.3}_{-0.2}$	$-17.7^{+0.3}_{-0.2}$	$-17.2^{+0.1}_{-0.1}$
NGC 6752	$-17.3^{+0.3}_{-0.4}$	$-17.0^{+0.4}_{-0.3}$	$-16.6^{+0.3}_{-0.2}$
NGC 7078	$-17.5^{+0.4}_{-0.2}$	$-17.4^{+0.4}_{-0.3}$	$-16.8^{+0.5}_{-0.3}$
NGC 7089	$-17.4^{+0.3}_{-0.2}$	$-17.3^{+0.3}_{-0.2}$	$-16.9^{+0.3}_{-0.2}$
NGC 7099	$-17.6^{+0.3}_{-0.2}$	$-17.4^{+0.3}_{-0.2}$	$-16.9^{+0.3}_{-0.2}$

3.4. Limiting flux

The results of the simulations above are now used to calculate the minimum amplitude of an emission line that can be detected. Since we select detections with a significance above 7.5, emission lines in spectra with too high noise will not be found. From the simulations, we first estimate the minimum signal-to-noise ratio SNR_{\min} for that 80 % of simulated emission lines are found. This SNR_{\min} depends on the width of the simulated emission line. Here, we chose a width of 40 Å, corresponding to cataclysmic variables. The minimum signal that we can detect is estimated by measuring the noise σ in the residuals of all spectra from 6000 Å to 7000 Å. In practice, the noise depends on the brightness of the target star, observing conditions, stellar crowding, etc. We measure this effective noise in the residuals obtained from the spectral fitting. The minimum detectable signal in each

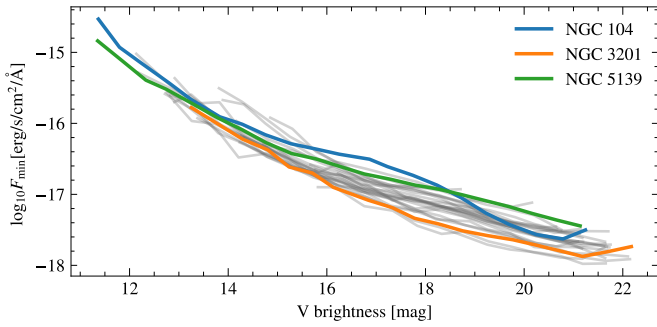


Fig. 3. Limiting flux for which 80 % of sources will be detected as determined from simulated emission lines for different clusters as a function of brightness. Each grey curve represents a GC, the clusters NGC 104, NGC 3201, and NGC 5139 are highlighted.

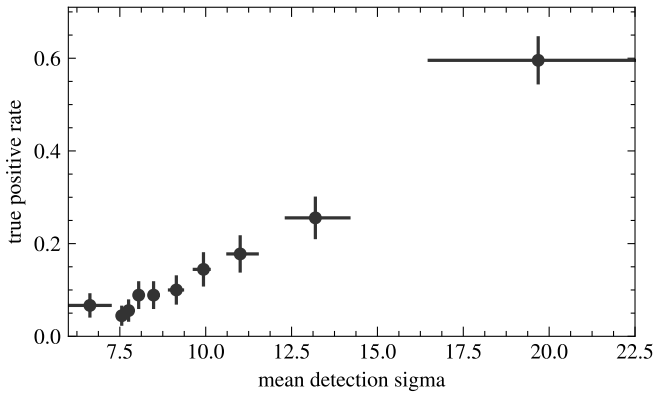


Fig. 4. Empirical true positive rate of matched filtering after checking about 1200 stars with detected emission lines. Each bin contains 90 stars and the errorbars contain the central 1σ interval of the detection significance per bin.

spectrum is $F_{\min} = \text{SNR}_{\min} \cdot \sigma$. Table 2 lists F_{\min} of a broad emission line for different representative points in the stellar population of each cluster we observed, and Fig. 3 shows the limiting flux as a function of stellar brightness in three clusters. Since we use a SNR_{\min} for which 80 % of simulated emission lines are found, Table 2 gives the limiting flux for which 80 % of all spectra with an emission line are found. Because we use a narrow filter width of 5 \AA to detect emission lines, the limits given for a broad emission line can be treated as a conservative estimate of the limiting flux of narrow emission lines. The limiting fluxes for narrow emission lines generally fall inside the uncertainties given in Table 2, this means that this table is also valid for narrow lines. Depending on the brightness of the target star, we find that F_{\min} is generally between $10^{-17} \dots 10^{-16} \text{ erg/s/cm}^2/\text{\AA}$. To our knowledge, this is the first optical emission-line survey estimating the upper limit of fluxes for sources that remain undetected.

4. The catalogue of emission-line sources

4.1. Results of visual inspection

We applied both detection methods to spectra extracted from MUSE observations of globular clusters (see Sect. 2.1) that have a signal-to-noise-ratio of at least five. Setting this threshold ensures that the spectral fit gives meaningful residuals. We want to

inspect promising emission-line spectra visually. As this would be very time consuming with thousands of candidate spectra, we check candidate spectra which contain an emission line close to $\text{H}\alpha$ (between 6540 and 6580 \AA) if $D_s > 7.5$. With this set-up, we expect to find emission-line stars, typically $\text{H}\alpha$ emitters, while galaxies would remain undetected. Section 4.7 describes how we find galaxies using all detected emission lines. In total, 1200 individual stars have at least one such spectrum, with a total of about 9000 spectra.

For each spectrum, we check if the emission line could be valid according to a set of criteria. The potential emission line has to be at least two pixels wide (a pixel corresponds to 1.25 \AA) and it must fulfill at least one of the following criteria:

- The line candidate appears in roughly the same position with the same shape in multiple spectra of the same star, or
- the spectrum shows emission lines in addition to $\text{H}\alpha$, or
- the corresponding star is listed in the *Catalogue of Variable Stars in Galactic Globular Clusters* (CVSGGC, Clement et al. 2001; Clement 2017), Simbad (Wenger et al. 2000), or in a suitable catalogue in VizieR (Ochsenbein et al. 2000), or
- the star is close to an X-ray source as listed in the Chandra Source Catalog Release 2.0 (Evans et al. 2010).

Typically, an emission-line candidate is not valid if the spectrum seems to be contaminated by other stars or nebulae. This occurs if a much brighter star is close ($\approx 2''$ or less) to the target star, or if it is close to one of the three nebulae in our survey.

Inspection of the results show that false positives are mainly caused by noise, contamination by brighter stars, and poor fit results. Figure 4 shows the empirical true positive rate after a visual check of each star with $D_s > 7.5$. For testing purposes, we also checked emission-line candidates with a lower significance than 7.5, these stars are also included in this figure. As expected, the true positive rate correlates with the mean detection significance and reaches about 60 % for $D_s > 6$.

Table A.2 lists all stars with spectra containing valid emission lines that we found in our survey. This table also gives the original ID used in the ACS catalogue in column ‘ACS ID’. The columns ‘ d_c ’ lists the projected distance to the respective cluster centre. The table also contains our estimate whether the star is a likely cluster member in column ‘mem.’. In contrast to Kamann et al. (2018), this estimate is based on radial velocities only. Column ‘ $v_{\text{rad}}?$ ’ contains an indicator whether the star shows variations in its radial velocity based on the method described in Giesers et al. (2019). We converted the probability of variability calculated in Giesers et al. (2019) in the following way: $p < 0.15$: not variable, $p > 0.85$: variable, $0.15 < p < 0.86$: unsure (?). Blank fields indicate insufficient data. We expect a false positive rate of 15 %. Cross-matches with other catalogues and papers are given in column ‘Ident.’ with the corresponding reference in column ‘Ref.’. The column ‘ d_x ’ contains the separation to the next Chandra X-ray source (Evans et al. 2010), if it is less than the positional uncertainties of the X-ray source. Background galaxies are listed in Table 3.

4.2. Cataclysmic variables

As described above, cataclysmic variables (CVs) are binary systems consisting of a hot, compact white dwarf and a dwarf star in a close orbit. Only ten CVs have been confirmed by spectroscopy in the whole globular cluster system of the Milky Way (Knigge 2012; Webb & Servillat 2013). Most CV candidates

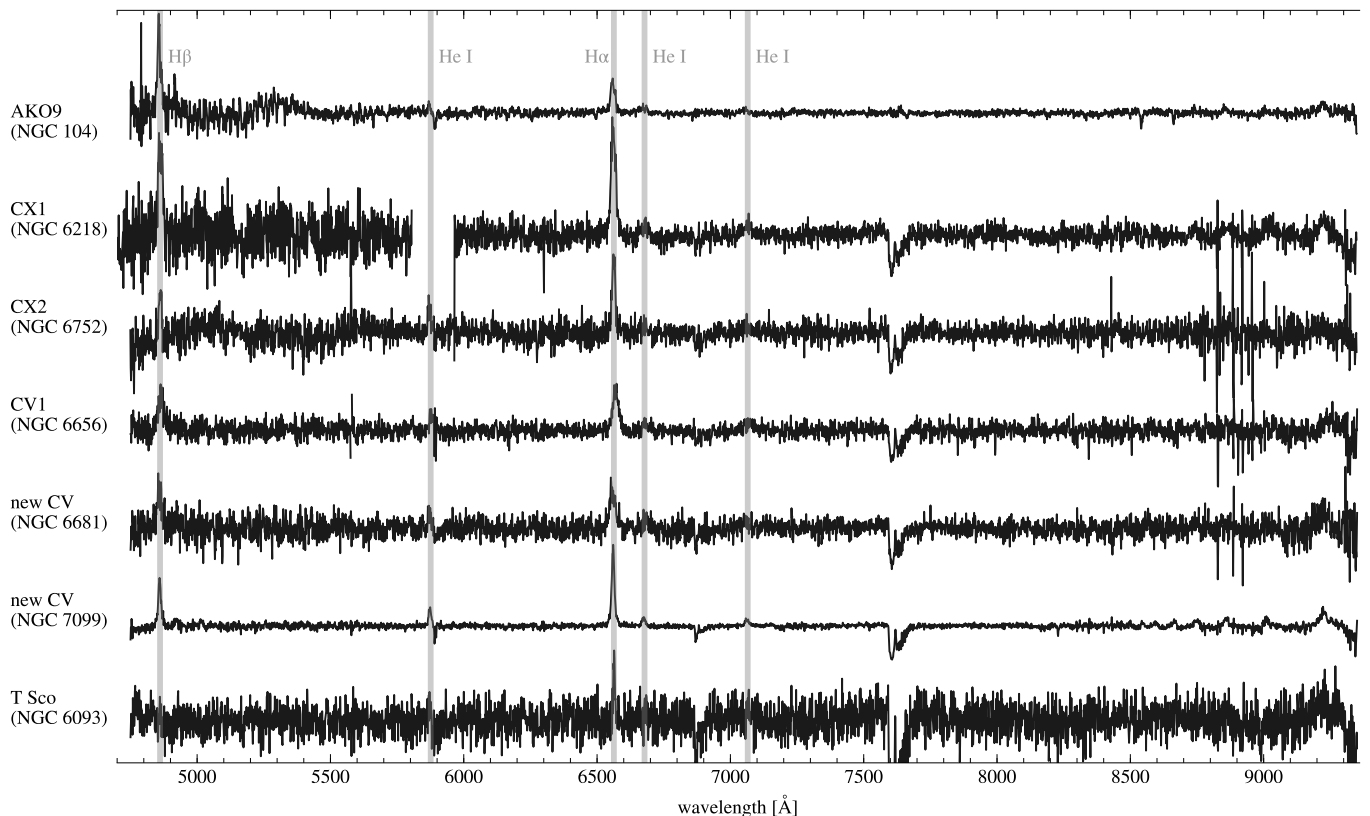


Fig. 5. Normalised spectra of known cataclysmic variables AKO9, CX1, CX2, CV1, of the new CVs in NGC 6681 and NGC 7099, and of the CV underlying the Nova T Sco in 1860. All spectra are detected by their broad Balmer emission lines, they also show He I emission. The spectrum shown for AKO9 was created by combining several observed spectra.

identified by photometry are not bright enough to be observed with MUSE and our relatively short exposure times. For example, Sandoval et al. (2018) lists R_{625} magnitudes for 21 CV candidates in NGC 104 of which only four are brighter than 20 mag.

4.2.1. Known CVs and confirming CV candidates

We find nine cataclysmic variables (CVs), of which seven are either previously spectroscopically confirmed CVs or candidates. The normalised MUSE spectra of several CVs including the previously unknown ones are shown in Fig. 5. Characteristic broad Balmer emission lines of $H\alpha$ and $H\beta$ are clearly visible in all spectra, as well as He I emission.

One of them, CX1 in NGC 6218 was detected as an X-ray source with optical counterpart and classified as a CV by Lu et al. (2009a) who consider it to be a member of the cluster based on its X-ray luminosity. We find that its optical counterpart is not the star marked in their finding chart but rather the star directly to the East with a F606W magnitude of 20.8. With this new counterpart, we can confirm that CX1 is indeed a CV.

We do not see the characteristic broad Balmer emission lines for a CV in any spectrum of W56/X6 in NGC 104 which was classified as a CV in Heinke et al. (2005). However, the spectra show a $H\alpha$ absorption line that is less deep than our spectral model predicts. Since this is not clearly a CV, we do not include it in our discussion in Section 5.1.

4.2.2. Nova T Scorpii

In 1860, a classical nova in NGC 6093 was observed by Pogson (1860), Nova T Scorpii. Both Shara & Drissen (1995) and Dieball et al. (2010) looked for the underlying CV using near- and far-UV observations and they found a UV bright source at the right spatial position. Using the finding charts in Dieball et al. (2010), we can identify their source 2129 with ACS ID 44184 ($F336W - F438W = -0.1$, $F438W = 18.5$, Piotto et al. 2015; Soto et al. 2017). This star was independently detected by our algorithm because of its broad $H\alpha$ emission in several of its ten spectra observed with MUSE. A visual inspection shows that also $H\beta$ and a weak He I emission are present and variable. The $H\alpha$ and $H\beta$ lines seem to switch between emission and absorption. However, as ACS ID 44184 is located on the lower RGB in the optical CMD, the CV has either a giant donor star or it is not resolved in the HST photometry but instead blended with an unrelated star.

4.2.3. New cataclysmic variables

Additionally to the seven known CVs, we find two more stars with very similar emission lines, indicating that these two stars are CVs as well. One new CV is close to the centre of NGC 7099 with a distance of $11''$ and a F606W magnitude of 20.3 in the ACS catalogue (ACS ID 23423). Based on its position close to an X-ray source and its blue $U - V$ colour, Lugger et al. (2007) identified this star as a possible CV candidate (source C). How-

ever, it is not included as a CV in the CVSGGC, which is why we list it as a new CV here.

The new CV in NGC 6681 (ACS ID 19706) has a distance of $27''$ to the cluster centre and a F606W magnitude of 22.7. The spectra of the new and known CVs are shown in Fig. 5. Both new CVs are close (0.13 and $0.25''$, respectively) to a Chandra X-ray source listed in the November 2017 pre-release of the Chandra Source Catalog Release 2.0 (Evans et al. 2010). Although NGC 6681 was observed with HST in the UV (see e.g. Mas-sari et al. 2013) and with the Chandra X-ray observatory (Pooley 2007; Dieball 2008), no articles about CVs in this cluster have been published.

Are these CVs actually part of their respective cluster? In general, we use the radial velocity and metallicity to determine if a star is a member of a globular cluster or a field star. The standard spectral fit fails to determine reliable radial velocities or metallicities from the spectra of the new CVs. We use a Gaussian fit to the $H\alpha$ line to estimate the radial velocity for each CV, including the known CVs. The velocities differ from the cluster values by up to 300 km/s. This could be because the emission lines in some cases seem to have a more complex, that is non-gaussian, shape, or because of intrinsically high velocity variations due to the orbital motions, or possibly because of eclipses of the accretion disk as observed for AKO9 (Knigge et al. 2003).

We assume that CVs in GCs are spatially distributed in the same way as all other stars in a GC. In the simulations of Belloni et al. (2019), CVs are either distributed more centrally or in the same way as main-sequence stars, depending on the relation time of the GCs. With this property of CVs, we can also use Bayes factors to decide between the two hypotheses $A \equiv$ “CV is a cluster member” and $B \equiv$ “CV is not a cluster member”. To calculate the factors we make use of the spatial distribution and membership probability derived from the observed radial velocity and metallicity of all the other stars observed with MUSE in the same field of view (see Kamann et al. 2018 for details). The distances of the new CVs to the respective cluster centre are about $1/6$ of the half-light radius (NGC 7099) and $2/3$ (NGC 6681) when the values from Harris (1996) are used. In the MUSE FOV of NGC 7099 96 % of all stars are cluster members; this leaves about 4 % non-members. Of all member stars, 8 % are closer to the cluster centre than the CV we consider, while the remaining 92 % are farther away. Thus, the likelihood of being a member star and at the same separation from the cluster centre or even closer is $p_A = 0.074$. As for non-members, 10 % lie closer to the centre than the CV, and 90 % are farther away. This gives $p_B = 0.004$. The Bayes factor is $p_A/p_B \approx 18$, which means that the positions of the CV provide evidence in favor of hypothesis A. The same analysis for the CV that may be associated with NGC 6681 gives a Bayes factor of $p_A/p_B \approx 13$. Here, 92 % are member stars, of which two third lie closer to the centre than the CV. Of the 8 % non-members, 55 % lie closer to the centre. According to the interpretation of Jeffreys (1998, p. 432), Bayes factors between 10 and $10^{3/2}$ provide *strong* evidence in favor of hypothesis A. In conclusion, the positions of the CVs and all the other stars in the MUSE FOV strongly suggest that both CVs are members of the respective cluster.

4.3. Optical counterpart of M62-VLA1

Several stellar mass black holes or candidates are known in globular clusters, including three in NGC 3201 (Giesers et al. 2018, 2019), M22-VLA1 and -VLA2 in NGC 6656 (Strader et al. 2012), and M62-VLA1 in NGC 6266 (Chomiuk et al. 2013). The black-hole candidates in NGC 3201 was discovered by Giesers

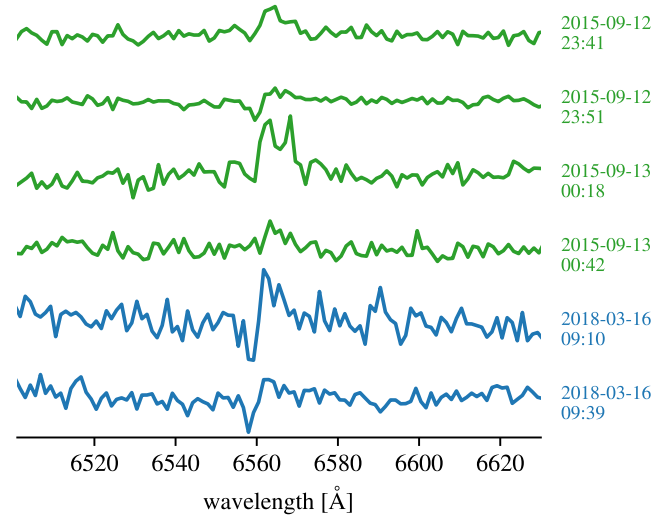


Fig. 6. $H\alpha$ region of multiple spectra of the likely companion of the black-hole candidate M62-VLA1. This part of the spectrum is variable on the timescale of minutes.

et al. (2018) and Giesers et al. (2019) using variations in the radial velocities of its visible companion observed with MUSE. These discoveries demonstrate that MUSE observations can be used to detect stellar exotica in GCs.

The black-hole candidate M62-VLA1 is close to the centre of NGC 6266 and was discovered by Strader et al. (2012) using radio and X-ray observations. It is likely to be part of a binary system with a star on the lower red-giant branch, which the authors identified in HST images very close to their radio source. Our emission-line search found the optical counterpart of this black hole because of its $H\alpha$ emission line. Both the position of this star and the counterpart reported in Strader et al. (2012) match, as well as the location in the colour-magnitude diagram. This star has been observed several times with MUSE in 2015 and again in 2018 with varying signal-to-noise. The spectra with the highest signal-to-noise show a $H\alpha$ emission line which seem to vary between observations. These variations in the $H\alpha$ region are shown in Fig. 6 where the shape of the emission line changes within tens of minutes. We need more observations to determine reliable orbital parameters for this system similarly to the black holes and the 92 other binary systems in NGC 3201 (Giesers et al. 2019).

4.4. Red stragglers and sub-subgiants

Red stragglers (RS) and sub-subgiants (SSG) are stars in globular clusters that occupy the region redwards of the red-giant branch or below the subgiant branch in the CMD. Since stellar evolution theory predicts these regions to be empty, their existence needs to be explained by more complicated formation theories (Geller et al. 2017a; Leiner et al. 2017; Geller et al. 2017b). Besides their location in the CMD, RS are X-ray and $H\alpha$ emitters, photometrically variable and mostly radial-velocity binaries (Geller et al. 2017a). As expected, several detected emission-line stars fall into the CMD region occupied by RS (four stars) and SSG (12 stars, see column ‘ID’ in Table A.2). In particular, we detect the RS binary in NGC 6254 discovered by Shishkovsky et al. (2018) which is also a source of radio and X-ray radi-

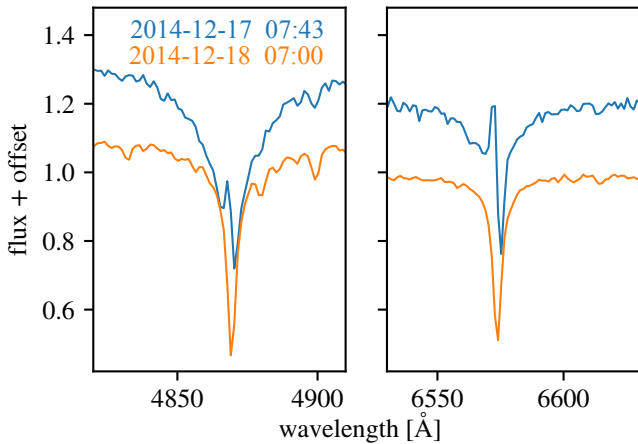


Fig. 7. Two spectra of the RR Lyrae star NGC3201-V90 (CVSGGC) observed approximately 24 hours apart show very different Balmer profiles. $H\alpha$ and $H\beta$ emission is only observed in one of the spectra, but not in the other one.

tion. A similar case is a star (ACS ID 40733) in the RS region of NGC 6541 which has a very broad and variable $H\alpha$ emission, and it is close to an X-ray source ($0''.18$). Of the eleven SSG that show $H\alpha$ emission and are probable cluster members, eight are close to an X-ray source, eight show variations in their radial velocities, and seven SSG are both close to an X-ray source and have radial velocity variations. All four RS with $H\alpha$ emission are members of their respective cluster, three are close to an X-ray source and those three RS also show radial velocity variations. We do not detect variability in the radial velocities of the fourth RS and it is not associated with an X-ray source. These correlations fit the general characteristics of SSG and RS as described in Geller et al. (2017a). Orbital parameters for several SSG systems in NGC 3201, including the $H\alpha$ emitters discovered here, are presented in Giesers et al. (2019).

4.5. Pulsating variables

About 40 % of all emission-line stars found in this survey are already known pulsating variable stars including W Virginis variables, slow irregular variables, long-period variables, semiregular variables, and RR Lyrae variables. Spectra of these stars show constant or variable $H\alpha$ and sometimes $H\beta$ emission fluxes.

Since the work of Struve (1947) it is known that spectra of RR Lyrae stars have a varying, weak emission component in several Hydrogen lines. Figure 7 shows two spectra of the RR Lyrae star V90 in NGC 3201 as an example of variable emission lines. The two spectra were observed roughly 24 hours apart and only the earlier one shows $H\alpha$ and $H\beta$ emission lines. The flux profiles are very similar to the first or second apparition of the RR Lyr variable X Ari shown in Gillet & Fokin (2014) in Fig. 1. The variable star V13 and possibly also V190 in NGC 6266 are currently classified as RR Lyrae stars in the literature. However, their spectra show very strong $H\alpha$ and $H\beta$ emission lines, similar to those of W Virginis variables.

4.6. Known nebulae

There are four known planetary nebulae (PNe) in the whole globular cluster system of the Milky Way. These are Ps 1 in NGC 7078 (Pease 1928), GJJC-1 in NGC 6656 (Gillett et al.

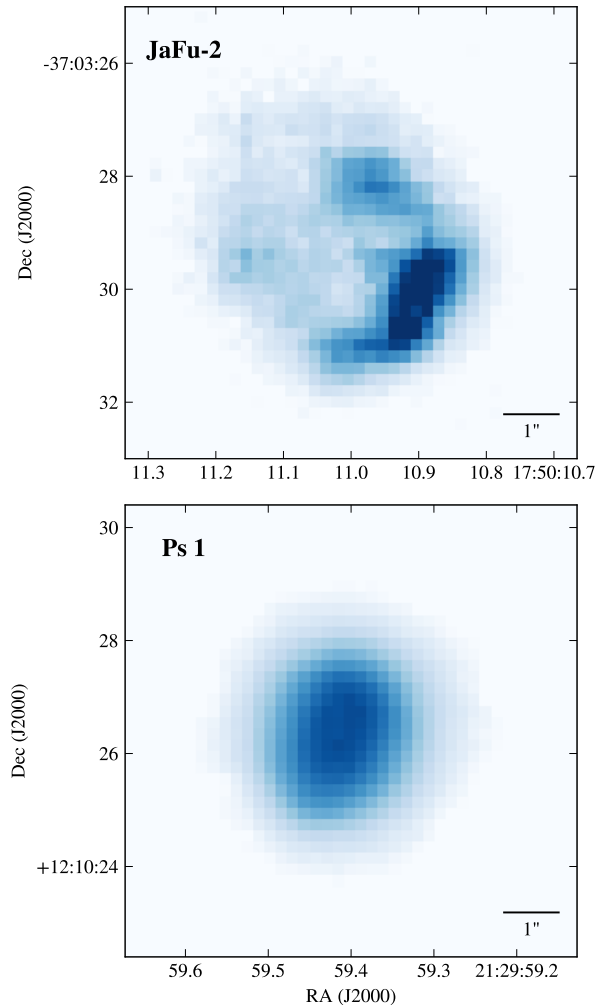


Fig. 8. Flux maps of the two known planetary nebulae in our sample: JaFu-2 (top) in NGC 6441 and Ps 1 (bottom) in NGC 7078. Shown is the $[O\text{ III}]\lambda 5007$ flux after the stellar background has been subtracted.

1989), JaFu-1 in Pal 6, and JaFu-2 in NGC 6441 (both Jacoby et al. 1997).

The most successful and also largest survey of PNe in globular clusters is the one from Jacoby et al. (1997), who used the on-band/off-band technique at the $[O\text{ III}]$ line at 5007 Å on 133 globular clusters. With this survey, they doubled the number of known PNe in GCs from two to four.

Of the four globular clusters with known PNe, Pal 6 is not included in our sample of GCs. Although our survey covers NGC 6656, GJJC-1 is not inside the MUSE FOV because of its position inside the cluster. This leaves Ps 1 and JaFu-2 for which we provide flux maps and spectra. Figure 8 shows $[O\text{ III}]$ maps of the two PNe side-by-side, the PN spectra are shown in Fig. 9. The spectra were extracted with a relatively large circular aperture covering the whole nebula. Although the nebulae are not HST point sources and, accordingly, we do not automatically extract a spectrum at their positions, the detection algorithm finds the nebular emission lines. This is because their emission flux contaminates the otherwise purely stellar spectra of dozens of nearby stars as its high spatial variability is not accounted for in the extraction.

In addition to these two planetary nebulae, we detected a nova remnant in NGC 6656 which is described in detail in

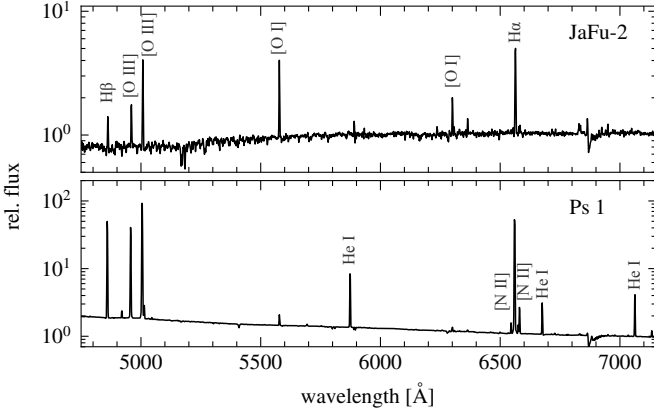


Fig. 9. Spectra of JaFu-2 (top) and Ps 1 (bottom). Prominent emission lines of Hydrogen, He I, [N II], [O I] and [O III] are labelled.

Table 3. Positions and redshifts of background galaxies with emission lines. The projected angular separation to the cluster centre is d_c .

Cluster	RA [°]	Dec [°]	d_c ["]	z
NGC 104	5.97861	-72.10556	100.6	0.330
NGC 104	6.05634	-72.05887	88.4	0.472
NGC 1851	78.52291	-40.03877	31.5	0.309
NGC 1851	78.53530	-40.03363	50.5	0.633
NGC 5139	201.66150	-47.40166	293.4	0.144
NGC 5139	201.66193	-47.39549	314.4	0.052
NGC 5904	229.61804	2.06133	102.0	0.414
NGC 6266	255.29045	-30.10210	58.0	0.722
NGC 6388	264.07237	-44.73578	1.8	0.420
NGC 6541	272.02490	-43.70413	55.1	0.413
NGC 6681	280.79848	-32.28750	21.9	0.305
NGC 6681	280.79929	-32.29805	24.4	0.173
NGC 6752	287.66226	-59.98960	100.4	0.364
NGC 6752	287.69412	-59.96586	79.0	0.312
NGC 6752	287.69667	-59.96068	93.5	0.246
NGC 6752	287.72543	-60.01487	110.1	0.505
NGC 6752	287.77154	-59.98476	98.0	0.105
NGC 7078	322.49858	12.17520	35.4	0.261
NGC 7078	322.50275	12.15647	51.0	0.670
NGC 7089	323.37114	-0.82728	34.0	0.737
NGC 7099	325.09295	-23.17880	4.6	0.398

Göttgens et al. (2019). However, we did not find any additional nebulae in our observations. We checked this null-result by stacking cubes from different observations to increase our sensitivity. We used the on-band/off-band technique around $H\alpha$ to search for extended emitting regions and did not find any nebula.

4.7. Galaxies

For each spectrum, we use the full list of emission-line candidates and their wavelengths to check if they correspond to a list of typical galactic emission lines, assuming they all have the same redshift. Using this method, we find 21 background galaxies that contaminate spectra we have extracted at known stellar positions in observations of several GCs (see Table 3). Since these spectra contain the stellar $H\alpha$ absorption line, we conclude that these are indeed blended spectra of a star and a background galaxy. The spectra are identified by their prominent emission

lines of Hydrogen and ionised Oxygen, as shown in Fig. 10 for three examples. We detect emission lines corresponding to rest-frame wavelengths of 3727 Å from [O II], of 4959 Å and 5007 Å from [O III], and $H\beta$ and $H\alpha$ emission. Table 3 lists the position, the redshift calculated from the emission lines, and the projected angular separation to the cluster centre for each galaxy. Because of the low [N II] to $H\alpha$ flux, all galaxies fall into the region occupied by starburst galaxies in the BPT diagram (Baldwin et al. 1981; Veilleux & Osterbrock 1987), except for one galaxy behind NGC 6752 at $z = 0.364$ which lies at the border of Seyfert galaxies and LINER. Deeper photometric observations of the fields containing the new galaxies may identify the counterparts which could be used to convert relative stellar proper motions into absolute proper motions, as done for NGC 6681 using HST images (Massari et al. 2013). These serendipitous discoveries resemble the one reported by Bedin et al. (2019), who found a dwarf spheroidal galaxy behind the globular cluster NGC 6752 using HST photometry. The fact that a galaxy lies very close to the core of the core-collapsed cluster NGC 7099 shows our capability to look through the GCs.

4.8. Unidentified sources

We find several emission-line stars that lie close to known X-ray sources. As a reference, we use the November 2017 pre-release of the Chandra Source Catalog Release 2.0 (Evans et al. 2010), which includes positions and error ellipses (including astrometric uncertainties) for X-ray sources in all but two clusters in our survey (NGC 6254 and NGC 6624). Based on the source positions and the associated errors, we estimated that there is no physical relation between a star and an X-ray source if their distance is $> 1''$. In general, multiple stars have a distance lower than $1''$ to an X-ray source which prohibits a unique identification of the optical counterpart. However, because both emission-line sources and X-ray sources are rare objects in globular clusters, we indicate if an X-ray source is close in the Table A.2.

As indicated in Table A.2, some stars show variable $H\alpha$ emission wings or asymmetric absorption. In the case of giant stars, these features could point to chromospheric activity or mass motions (e.g. Cohen 1976; Cacciari et al. 2004; Meszaros et al. 2008).

5. Discussion and conclusions

5.1. Completeness of the extraction of stellar sources

There are two steps in the detection of emission-line sources in MUSE data that influence how many existing sources can be found: the extraction completeness and the efficiency of matched filtering. We discuss only the first one here, the second one was described in Sect. 3.3.

The extraction completeness is the ratio of ACS catalogue sources for which a spectrum can be extracted from the MUSE datacube to all sources in the MUSE field of view. Figure 11 shows the dependence of our extraction completeness for all clusters taking all spectra with a SNR better than five into account. An extraction completeness of 100 % does not mean that we have a spectrum of all stars in our FOV but only of those listed in the ACS catalogue. This is an important distinction for low brightness stars in the central few arcseconds of core-collapsed clusters, such as NGC 7078. Thus we expect that the completeness depends not only on the brightness of a star but also on its position relative to the cluster centre (see Fig. A.1).

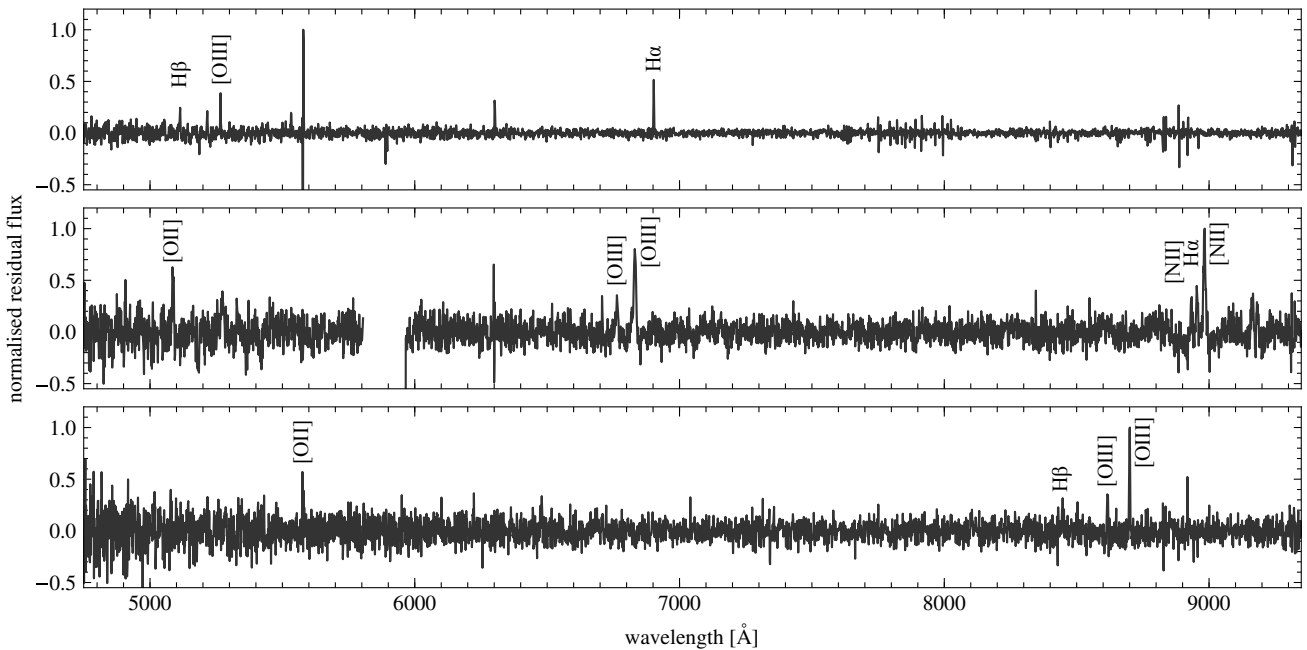


Fig. 10. Normalised residuals of stellar spectra that contain extragalactic emission lines including from [O II], [O III], and H I. Redshifts determined from these lines are $z = 0.05, 0.36$ and 0.737 , respectively. The top and bottom panels show a starburst galaxy, while the middle panel shows an AGN.

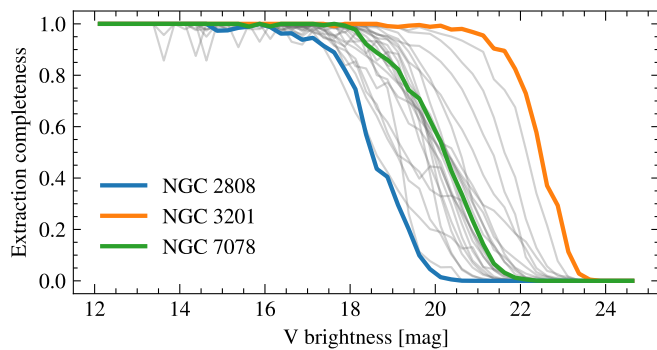


Fig. 11. Spectral extraction completeness (SNR > 5) for all clusters with respect to the ACS catalogue as a function of brightness (filters are listed in Table 4). Each grey curve represents a single cluster, the curves for NGC 2808, NGC 3201, and NGC 7078 are highlighted. Since the completeness mainly depends on the stellar density, it also depends on the radial distance to the cluster centre (see Fig. A.1 in the appendix).

We estimate the extraction completeness for different magnitudes and for three regions: the whole FOV, the central $10''$, the intermediate region from $10''$ to $60''$ and the remaining outer regions. Figure A.1 in the Appendix shows how our extraction completeness depends on the brightness of the star and its position in the case of NGC 7078. In general we see a completeness of close to 100 % for bright stars throughout the cluster. The crowded cluster centre hinders the extraction of faint sources and the completeness starts to drop below 50 % for magnitudes between 18 and 19 mag for most clusters.

5.2. Do we find enough CVs?

Massive globular clusters are expected to host about 200 CVs (Ivanova et al. 2006; Knigge 2012). However, the cluster with the most CV candidates, as determined by UV and optical photometry and X-ray data, is NGC 104 with 43 CVs (Sandoval et al. 2018). In contrast, the number of spectroscopically confirmed CVs is much lower: only ten CVs have been confirmed by spectroscopy in the whole globular cluster system of the Milky Way (Knigge 2012; Webb & Servillat 2013). We add seven CVs to this list, including two newly detected CVs. CVs in globular clusters are hard to observe by spectroscopy because of the low brightness of the secondary component and crowding. We expect to find dwarf novae (DNe), a subtype of CVs, because they have spectra with emission lines in quiescence (Clarke et al. 1984; Warner 1995) and observations show that most CVs are DNe (Knigge et al. 2011). Is our number of CV detections consistent with the prediction? To answer this question, we use the average CV brightness distribution from MOCCA simulations of globular clusters (Belloni et al. 2016). We did not consider effects of incomplete spatial coverage in our survey, because most CVs are expected to be located inside the half-mass radius of the respective cluster (Belloni et al. 2016, but also see Belloni et al. 2019). For each cluster, we draw samples from this distribution and use our completeness function and a detection probability of 80 % (Sect. 3.3) to estimate the number of CVs for which we should have extracted spectra (see Table A.1 in the Appendix). Since the clusters differ in their structural parameters and Belloni et al. (2016) give a CV brightness distribution for an average globular cluster, the number of CVs for each individual cluster is probably not meaningful. The total number of expected CV detections using the model of Belloni et al. (2016) in our sample is 10 ± 2 , which is consistent with our number of nine detected CVs.

The step that restricts the overall completeness for CVs the most is the extraction completeness at magnitudes of 22 and be-

low. This could be improved with longer observations using the narrow-field mode (NFM) of MUSE, which will offer a much higher spatial sampling in a smaller FOV.

5.3. Exclusion of more PNe

While the limiting fluxes given in Table 2 are, if interpreted strictly, only valid for emission in stellar spectra, we can rule out any large diffuse source of H α emission lines in our fields of view. Any nebula or other diffuse source of emission would need to overlap with at least some stars of which we extracted spectra. In the same way we easily detected JaFu-2, Ps 1, and the nova remnant in NGC 6656 (Göttgens et al. 2019), these contaminated spectra would have been found.

There are still some possible but unlikely ways a hypothetical PNe could be hidden in a GC: It could be very small so that it only contaminates a few stars, ideally of low brightness. In this case, we might not extract a spectrum for them. The maximum size of this nebula cannot be large, considering the high density of sources for which we can extract spectra. Another possibility is a nebula with very faint H α emission that would have to be much fainter than the known ones because those were easily found with our detection method.

However, it is still possible that more nebulae similar to the nova in NGC 6656 lie outside the area covered by our survey. In this case, it has to be in a region of relatively high stellar density where it can not be detected by photometric surveys.

6. Summary

We analysed data from our MUSE survey of 26 Galactic globular clusters, looking for signs of emission-line objects. Taking advantage of previous work on the same data, including data reduction, spectra extraction, and spectral analysis, we found 156 emission-line stars and several non-stellar emission-line sources. By assuming a Gaussian emission-line shape and using matched filtering, we detect this shape in the residuals generated during a full spectrum fit to the observed spectra. Since this generates many potentially interesting emission-line candidates, we use a threshold to select only the most promising candidates and check them visually. We did not use external catalogues to search for known sources in our data, but we used them to validate and categorise our findings. We found two new cataclysmic variables, many known pulsating variable stars, and several unidentified emission-line stars close to known X-ray sources. The total number of CVs detected in this survey is consistent with numerical simulations when our spectral extraction completeness is taken into account. In addition to stellar emission-line sources, we also found 20 previously unknown starburst galaxies and one AGN in the background with redshifts from 0.05 to 0.74.

Acknowledgements. FG, SK and SD acknowledge support from the German Research Foundation (DFG) through projects KA 4537/2-1 and DR 281/35-1. SK gratefully acknowledges funding from a European Research Council consolidator grant (ERC-CoG-646928- Multi-Pop). PMW, SK, SD and BG also acknowledge support from the German Ministry for Education and Science (BMBF Verbundforschung) through projects MUSE-AO, grants 05A14BAC and 05A14MGA, and MUSE-NFM, grants 05A17MGA and 05A17BAA. Based on observations made with ESO Telescopes at the La Silla Paranal Observatory under programme IDs 094.D-0142, 095.D-0629, 096.D-0175, 097.D-0295, 098.D-0148, 099.D-0019, 0100.D-0161, 0101.D-0268, and 0102.D-0270. Also based on observations made with the NASA/ESA Hubble Space Telescope, obtained from the data archive at the Space Telescope Science Institute. STScI is operated by the Association of Universities for Research in Astronomy, Inc. under NASA contract NAS 5-26555.

Table 4. Choice of V filter for each cluster used in this paper.

ACS/WFC3 filter	Clusters
F625W	NGC 6522
F555W	NGC 1904, NGC 6266, NGC 6293
F606W	NGC 104, NGC 1851, NGC 2808, NGC 3201 NGC 362, NGC 5139, NGC 5286, NGC 5904, NGC 6093, NGC 6121, NGC 6218, NGC 6254, NGC 6388, NGC 6441, NGC 6541, NGC 6624 NGC 6656, NGC 6681, NGC 6752, NGC 7078 NGC 7089, NGC 7099

References

- Abbott, B., Abbott, R., Abbott, T., et al. 2016, *Physical Review Letters*, 116, 061102
- Albrow, M. D., Gilliland, R. L., Brown, T. M., et al. 2001, *The Astrophysical Journal*, 559, 1060
- Anderson, J., Sarajedini, A., Bedin, L. R., et al. 2008, *The Astronomical Journal*, 135, 2055
- Askar, A., Sedda, M. A., & Giersz, M. 2018, *Monthly Notices of the Royal Astronomical Society*, 478, 1844, wOS:000439547400031
- Bacon, R., Accardo, M., Adjali, L., et al. 2010, in *Ground-based and Airborne Instrumentation for Astronomy III*, Vol. 7735 (International Society for Optics and Photonics), 773508
- Bacon, R., Conseil, S., Mary, D., et al. 2017, *Astronomy & Astrophysics*, 608, A1
- Baldwin, J. A., Phillips, M. M., & Terlevich, R. 1981, *Publications of the Astronomical Society of the Pacific*, 93, 5
- Bassa, C., Pooley, D., Homer, L., et al. 2004, *The Astrophysical Journal*, 609, 755
- Bedin, L. R., Salaris, M., Rich, R. M., et al. 2019, *Monthly Notices of the Royal Astronomical Society: Letters*, 484, L54
- Belloni, D., Giersz, M., Askar, A., Leigh, N., & Hypki, A. 2016, *Monthly Notices of the Royal Astronomical Society*, 462, 2950
- Belloni, D., Giersz, M., Rivera Sandoval, L. E., Askar, A., & Ciecieląg, P. 2019, *Monthly Notices of the Royal Astronomical Society*, 483, 315
- Cacciari, C., Bragaglia, A., Rossetti, E., et al. 2004, *Astronomy & Astrophysics*, 413, 343
- Campos, F., Pelisoli, I., Kamann, S., et al. 2018, *Monthly Notices of the Royal Astronomical Society*, 481, 4397
- Chomiuk, L., Strader, J., Maccarone, T. J., et al. 2013, *The Astrophysical Journal*, 777, 69
- Clarke, J. T., Capel, D., & Bowyer, S. 1984, *The Astrophysical Journal*, 287, 845
- Clement, C. 2017, *EPJ Web of Conferences*, 152, 01021
- Clement, C. M., Muzzin, A., Dufton, Q., et al. 2001, *The Astronomical Journal*, 122, 2587
- Cohen, J. G. 1976, *The Astrophysical Journal Letters*, 203, L127
- Cool, A. M., Haggard, D., Arias, T., et al. 2013, *The Astrophysical Journal*, 763, 126
- Dieball, A. 2008, *Chandra Proposal* 10300600
- Dieball, A., Long, K. S., Knigge, C., Thomson, G. S., & Zurek, D. R. 2010, *The Astrophysical Journal*, 710, 332
- Evans, I. N., Primini, F. A., Glotfelty, K. J., et al. 2010, *The Astrophysical Journal Supplement Series*, 189, 37
- Geller, A. M., Leiner, E. M., Bellini, A., et al. 2017a, *The Astrophysical Journal*, 840, 66
- Geller, A. M., Leiner, E. M., Chatterjee, S., et al. 2017b, *The Astrophysical Journal*, 842, 1
- Giesers, B., Dreizler, S., Husser, T.-O., et al. 2018, *Monthly Notices of the Royal Astronomical Society: Letters*, 475, L15
- Giesers, B., Kamann, S., Dreizler, S., et al. 2019, arXiv:1909.04050 [astro-ph], arXiv: 1909.04050
- Gillet, D. & Fokin, A. B. 2014, *Astronomy & Astrophysics*, 565, A73
- Gillet, F. C., Jacoby, G. H., Joyce, R. R., et al. 1989, *The Astrophysical Journal*, 338, 862
- Göttgens, F., Weilbacher, P. M., Roth, M. M., et al. 2019, *Astronomy & Astrophysics*, 626, A69
- Harris, W. E. 1996, *The Astronomical Journal*, 112, 1487
- Heinke, C. O., Grindlay, J. E., Edmonds, P. D., et al. 2005, *The Astrophysical Journal*, 625, 796
- Heinke, C. O., Grindlay, J. E., Edmonds, P. D., et al. 2003, *The Astrophysical Journal*, 598, 516
- Herenz, E. C. & Wisotzki, L. 2017, *Astronomy & Astrophysics*, 602, A111

- Husser, T.-O., Kamann, S., Dreizler, S., et al. 2016, *Astronomy & Astrophysics*, 588, A148
- Husser, T.-O., Wende-von Berg, S., Dreizler, S., et al. 2013, *Astronomy and Astrophysics*, 553, A6
- Ivanova, N., Heinke, C. O., Rasio, F. A., et al. 2006, *Monthly Notices of the Royal Astronomical Society*, 372, 1043
- Jacoby, G. H., Marco, O. D., Davies, J., et al. 2017, *The Astrophysical Journal*, 836, 93
- Jacoby, G. H., Morse, J. A., Fullton, L. K., Kwitter, K. B., & Henry, R. B. C. 1997, *The Astronomical Journal*, 114, 2611
- Jeffreys, H. 1998, *The Theory of Probability* (OUP Oxford)
- Kaluzny, J., Rozyczka, M., Thompson, I. B., et al. 2016, *Acta Astronomica*, 66, 31
- Kamann, S., Husser, T.-O., Dreizler, S., et al. 2018, *Monthly Notices of the Royal Astronomical Society*, 473, 5591
- Kamann, S., Wisotzki, L., & Roth, M. M. 2013, *Astronomy and Astrophysics*, 549, A71
- Knigge, C. 2012, *Mem.Soc.Ast.It.*, 83, 549
- Knigge, C., Baraffe, I., & Patterson, J. 2011, *The Astrophysical Journal Supplement Series*, 194, 28
- Knigge, C., Zurek, D. R., Shara, M. M., Long, K. S., & Gilliland, R. L. 2003, *The Astrophysical Journal*, 599, 1320
- Kremer, K., Ye, C. S., Chatterjee, S., Rodriguez, C. L., & Rasio, F. A. 2018, *Astrophysical Journal Letters*, 855, L15
- Kunder, A., Stetson, P. B., Catelan, M., Walker, A. R., & Amigo, P. 2013, *The Astronomical Journal*, 145, 33
- Lebzelter, T. & Wood, P. R. 2016, *Astronomy & Astrophysics*, 585, A111
- Leiner, E., Mathieu, R. D., & Geller, A. M. 2017, *The Astrophysical Journal*, 840, 67
- Lu, T.-N., Kong, A. K. H., Bassa, C., et al. 2009a, *The Astrophysical Journal*, 705, 175
- Lu, T.-N., Kong, A. K. H., Bassa, C., et al. 2009b, *The Astrophysical Journal*, 705, 175
- Lugger, P. M., Cohn, H. N., Cool, A. M., Heinke, C. O., & Anderson, J. 2017, *The Astrophysical Journal*, 841, 53
- Lugger, P. M., Cohn, H. N., Heinke, C. O., Grindlay, J. E., & Edmonds, P. D. 2007, *The Astrophysical Journal*, 657, 286
- Massari, D., Bellini, A., Ferraro, F. R., et al. 2013, *The Astrophysical Journal*, 779, 81
- Meszaros, S., Dupree, A. K., & Szentgyorgyi, A. 2008, *The Astronomical Journal*, 135, 1117
- Ochsenbein, F., Bauer, P., & Marcout, J. 2000, *Astronomy and Astrophysics Supplement Series*, 143, 23
- Pease, F. G. 1928, *Publications of the Astronomical Society of the Pacific*, 40, 342
- Piotto, G., Milone, A. P., Bedin, L. R., et al. 2015, *The Astronomical Journal*, 149, 91
- Pogson, N. 1860, *Monthly Notices of the Royal Astronomical Society*, 21, 32
- Pooley, D. 2007, *Chandra Proposal* 09300101
- Pooley, D., Lewin, W. H. G., Homer, L., et al. 2002, *The Astrophysical Journal*, 569, 405
- Ransom, S. M. 2007, *Proceedings of the International Astronomical Union*, 3, 291
- Roth, M. M., Sandin, C., Kamann, S., et al. 2018, *Astronomy & Astrophysics*, 618, A3
- Sandoval, R., E. L., van den Berg, M., et al. 2018, *Monthly Notices of the Royal Astronomical Society*, 475, 4841
- Sarajedini, A., Bedin, L. R., Chaboyer, B., et al. 2007, *The Astronomical Journal*, 133, 1658
- Shara, M. M. & Drissen, L. 1995, *The Astrophysical Journal*, 448, 203
- Shishkovsky, L., Strader, J., Chomiuk, L., et al. 2018, *The Astrophysical Journal*, 855, 55
- Soto, M., Bellini, A., Anderson, J., et al. 2017, *The Astronomical Journal*, 153, 19
- Strader, J., Chomiuk, L., Maccarone, T. J., Miller-Jones, J. C. A., & Seth, A. C. 2012, *Nature*, 490, 71
- Struve, O. 1947, *Publications of the Astronomical Society of the Pacific*, 59, 192
- Veilleux, S. & Osterbrock, D. E. 1987, *The Astrophysical Journal Supplement Series*, 63, 295
- Vio, R. & Andreani, P. 2016, *Astronomy & Astrophysics*, 589, A20
- Warner, B. 1995, in *Cataclysmic Variable Stars*, *Cambridge Astrophysics* (Cambridge University Press), 126–215
- Webb, N. A., Serre, D., Gendre, B., et al. 2004, *Astronomy & Astrophysics*, 424, 133
- Webb, N. A. & Servillat, M. 2013, *Astronomy & Astrophysics*, 551, A60
- Weilbacher, P. M., Streicher, O., Urrutia, T., et al. 2012, in *Software and Cyber-infrastructure for Astronomy II*, Vol. 8451 (International Society for Optics and Photonics), 84510B
- Weilbacher, P. M., Streicher, O., Urrutia, T., et al. 2014, in *ASP Conf. Ser.*, ed. N. Manset & P. Forshay, Vol. 485, 451
- Wendt, M., Husser, T.-O., Kamann, S., et al. 2017, *Astronomy & Astrophysics*, 607, A133
- Wenger, M., Ochsenbein, F., Egret, D., et al. 2000, *Astronomy and Astrophysics Supplement Series*, 143, 9

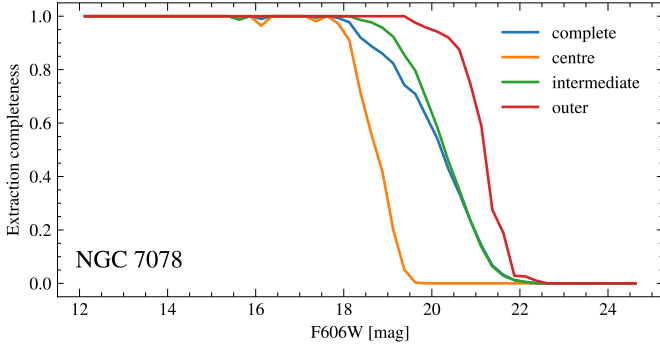


Fig. A.1. Spectral extraction completeness in NGC 7078 relative to the ACS catalogue. For this cluster, we reach a completeness of 50 % at a magnitude of 17, 20, and 21.5 for the central region (innermost 10''), an intermediate region (between 10'' and 60''), and the outer regions (outside 60''), respectively.

Appendix A: Completeness

Table A.1. Number of expected CVs in each cluster using the brightness distribution from Belloni et al. (2016). Columns ‘lower’ and ‘upper’ give the 1σ interval around the median value listed in column ‘median’. The column N_{found} refers to the number of spectroscopically detected CVs in our survey.

Cluster	lower	median	upper	N_{found}
NGC 3201	1.5	2.9	4.8	
NGC 6218	0.9	1.7	3.3	1
NGC 6254	0.8	1.6	2.9	
NGC 6656	0.5	1.3	2.1	1
NGC 6752	0.4	0.9	1.4	1
NGC 6121	0.1	0.3	0.9	
NGC 104	0.0	0.1	0.3	1
NGC 5904	0.0	0.1	0.3	
NGC 6681	0.0	0.1	0.3	1
NGC 7099	0.0	0.1	0.6	1
NGC 6266	0.0	0.0	0.2	
NGC 6624	0.0	0.0	0.2	
NGC 5139	0.0	0.0	0.2	1
NGC 6541	0.0	0.0	0.1	
NGC 5286	0.0	0.0	0.0	
NGC 6388	0.0	0.0	0.0	
NGC 6441	0.0	0.0	0.0	
NGC 7078	0.0	0.0	0.0	
NGC 6093	0.0	0.0	0.0	2
NGC 1851	0.0	0.0	0.0	
NGC 6293	0.0	0.0	0.0	
NGC 6522	0.0	0.0	0.0	
NGC 362	0.0	0.0	0.0	
NGC 2808	0.0	0.0	0.0	
NGC 1904	0.0	0.0	0.0	
NGC 7089	0.0	0.0	0.0	
total	8.1	10.0	12.5	9

Table A.2. Stars with spectra containing significant emission lines.

Cluster	RA	Dec	ACS ID	d_c ["]	V [mag]	mem.?	var?	d_x ["]	Comment	Ident.	Ref.
NGC 104	0 ^h 24 ^m 23 ^s 17	-72°5'42"06	22645	52.0	17.1	yes	?	0.12	variable, filled H α absorption	W56/X6 (CV)	1
NGC 104	0 ^h 24 ^m 42 ^s 21	-72°4'43"52	103550	11.3	16.9	yes		0.17	variable H α emission	(SSG)	
NGC 104	0 ^h 24 ^m 49 ^s 1	-72°4'55"53	59082	4.6	16.6	?		0.14	broad H α , H β and He emission	AKO9 (CV)	2
NGC 104	0 ^h 24 ^m 56 ^s 5	-72°5'42"21	58167	11.6	15.9	yes		0.15	noisy, filled H α absorption, contaminated?	W31 (MSP?)	1
NGC 104	0 ^h 24 ^m 66 ^s 1	-72°4'50"88	99987	4.7	15.5	yes	yes	0.36	variable H α emission	(SSG)	
NGC 104	0 ^h 24 ^m 85 ^s 5	-72°5'35"16	53591	44.6	17.0	yes	yes	0.19	noisy, variable, filled H α absorption	WF4-V04 (EA)	2
NGC 104	0 ^h 24 ^m 85 ^s 8	-72°3'54"83	136338	59.3	11.0	yes	no		variable H α , H β emission	V1 (SR)	2
NGC 104	0 ^h 24 ^m 13 ^s 76	-72°3'34"56	132746	86.5	17.2	yes	yes	0.20	variable, filled H α absorption	(SSG)	
NGC 104	0 ^h 24 ^m 15 ^s 16	-72°4'43"64	89607	44.7	17.0	yes	yes	0.14	variable H α emission	(RS)	3
NGC 104	0 ^h 24 ^m 17 ^s 23	-72°3'2"89	155735	122.0	17.0	yes	yes	0.10	filled H α absorption	(SSG?)	
NGC 362	1 ^h 3 ^m 12 ^s 77	-70°51'17"81	44740	23.4	17.8	yes	yes	0.09	variable H α emission	(SSG)	
NGC 362	1 ^h 3 ^m 14 ^s 42	-70°51'1"63	42163	6.1	16.0	yes	yes		filled H α absorption		
NGC 362	1 ^h 3 ^m 14 ^s 89	-70°51'28"46	41200	33.0	16.3	yes	yes	0.07	variable, filled H α absorption	(RS)	
NGC 362	1 ^h 3 ^m 15 ^s 08	-70°50'32"33	83177	23.6	11.8	yes	yes		variable H α , H β emission	V16 (Mira Ceti)	2
NGC 362	1 ^h 3 ^m 16 ^s 46	-70°50'55"96	39120	10.9	17.2	yes	yes	0.06	variable H α emission		
NGC 362	1 ^h 3 ^m 17 ^s 38	-70°50'37"67	79642	23.6	15.2	yes	yes		variable, filled H α absorption	Sz54 (RRLyr)	2
NGC 362	1 ^h 3 ^m 22 ^s 11	-70°50'44"76	73827	40.2	16.2	yes	yes	0.09	variable H α emission	V24 (EA)	2
NGC 1851	5 ^h 14 ^m 33 ^s 70	-40°3'5"46	58086	39.4	16.1	yes	yes		variable H α absorption	V27 (RRLyr)	2
NGC 1851	5 ^h 14 ^m 64 ^s 43	-40°2'48"66	96334	3.8	13.0	yes	?		variable H α absorption		
NGC 1851	5 ^h 14 ^m 84 ^s 48	-40°3'0"98	41019	24.0	19.6	yes			variable H α emission, contaminated?		
NGC 1851	5 ^h 14 ^m 85 ^s 4	-40°3'2"86	40603	25.6	19.0	yes			noisy, filled H α absorption	V4 (RRLyr)	2
NGC 1851	5 ^h 14 ^m 85 ^s 5	-40°2'16"98	87919	36.9	15.4	yes	yes		variable, filled H α absorption	V15 (RRLyr)	2
NGC 1851	5 ^h 14 ^m 90 ^s 9	-40°2'1"21	86191	53.6	16.2	yes	yes		variable, filled H α and H β absorption		
NGC 1851	5 ^h 14 ^m 99 ^s 4	-40°2'14"94	83855	49.0	18.9	yes	yes		variable H α emission		
NGC 1904	5 ^h 24 ^m 10 ^s 19	-24°31'2"45	250125	29.2	16.5	yes	yes		variable H α , H β absorption	V5 (RRLyr)	2
NGC 1904	5 ^h 24 ^m 11 ^s 48	-24°31'24"55	151206	7.0	14.6	yes			variable H α emission, contaminated?		
NGC 1904	5 ^h 24 ^m 11 ^s 49	-24°31'37"09	4	9.8	12.6	yes			H α and H β emission	V8 (SR)	2
NGC 1904	5 ^h 24 ^m 12 ^s 63	-24°31'40"94	80378	24.3	13.5	yes	yes		variable, filled H α absorption	V7 (W Vir)	2
NGC 2808	9 ^h 12 ^m 23 ^s 5	-64°52'4"42	106976	16.5	17.2	yes	yes		filled H α absorption?, between RGB and HB		
NGC 2808	9 ^h 12 ^m 35 ^s 1	-64°51'43"99	201163	5.3	12.5	yes	yes		variable H α emission		
NGC 2808	9 ^h 12 ^m 55 ^s 3	-64°51'31"01	194298	23.4	14.7	yes	yes		variable H α emission	V51 (BL Her)	4
NGC 2808	9 ^h 12 ^m 67 ^s 2	-64°52'40"30	26920	56.6	12.2	yes	no		variable H α emission	V11 (SR)	2
NGC 3201	10 ^h 17 ^m 32 ^s 62	-46°25'32"58	6558	64.4	14.7	yes	yes		variable, filled H α absorption	V23 (RRLyr)	2
NGC 3201	10 ^h 17 ^m 33 ^s 14	-46°25'7"42	14749	44.2	17.0	yes	yes		filled H α absorption	V141 (EA)	2
NGC 3201	10 ^h 17 ^m 34 ^s 89	-46°24'33"15	23979	23.1	14.4	yes	yes		variable H α , H β absorption	V90 (RRLyr)	2
NGC 3201	10 ^h 17 ^m 35 ^s 59	-46°24'50"51	13438	13.9	17.2	yes	yes	0.14	filled H α absorption	(SSG)	
NGC 3201	10 ^h 17 ^m 36 ^s 01	-46°25'12"50	13108	28.8	17.7	yes	yes		filled H α absorption	VN2 (EW)	5
NGC 3201	10 ^h 17 ^m 36 ^s 11	-46°25'36"03	5081	51.6	14.9	yes	yes		variable, filled H α absorption	V77 (RRLyr)	2
NGC 3201	10 ^h 17 ^m 36 ^s 14	-46°24'28"08	23379	18.2	14.9	yes	yes		variable, filled H α , H β absorption	V100 (RRLyr)	2
NGC 3201	10 ^h 17 ^m 37 ^s 58	-46°23'52"24	22692	53.2	17.3	yes	yes	0.06	variable H α emission	(SSG)	
NGC 3201	10 ^h 17 ^m 38 ^s 56	-46°24'27"12	22186	25.3	18.7	no	?	0.23	filled H α absorption		
NGC 3201	10 ^h 17 ^m 39 ^s 11	-46°24'30"11	21907	27.9	18.4	yes	yes		filled H α absorption, two spectral components	V135 (EW?)	2
NGC 3201	10 ^h 17 ^m 39 ^s 14	-46°24'11"03	21922	41.5	18.4	yes	yes		variable H α emission		
NGC 3201	10 ^h 17 ^m 39 ^s 25	-46°25'11"89	11405	36.9	17.3	yes	yes		filled H α absorption	(SSG)	
NGC 5139	13 ^h 26 ^m 32 ^s 57	-47°30'3"77	2036152	167.5	19.7 ^a	yes	yes		filled H α absorption		
NGC 5139	13 ^h 26 ^m 42 ^s 55	-47°24'21"87	1000193	268.9	14.2 ^a	yes	yes		variable filled H α absorption	V51 (RRLyr)	2
NGC 5139	13 ^h 26 ^m 43 ^s 30	-47°28'16"33	210583	50.0	18.7	yes		0.22	variable H α emission		

Table A.2. cont.

Cluster	RA	Dec	ACS ID	d_c ["]	V [mag]	mem.?	vrad?	d_X ["]	Comment	Ident.	Ref.
NGC 5139	13 ^h 26 ^m 43.361	-47°29'38".37	66994	63.6	11.0	yes	yes		variable H α emission	LW10 (LPV)	6
NGC 5139	13 ^h 26 ^m 44.32	-47°29'5".23	113810	35.0	11.3	yes	yes		variable H α emission	LW11 (LPV)	6
NGC 5139	13 ^h 26 ^m 46.36	-47°29'30".51	65282	44.9	13.3	?	no		variable H α , H β emission	V42 (SR)	2
NGC 5139	13 ^h 26 ^m 47.72	-47°29'29".00	64316	42.8	11.1	yes	?		variable H α emission	V152 (SR)	2
NGC 5139	13 ^h 26 ^m 53.51	-47°29'0".24	125876	65.1	20.0	yes		0.15	broad H α emission	13a (CV)	7
NGC 5139	13 ^h 26 ^m 55.04	-47°28'44".63	149184	79.1	18.9	yes	yes		filled H α absorption		
NGC 5286	13 ^h 46 ^m 24.86	-51°22'56".89	80568	34.8	13.0	yes			broad H α emission, but close to detector edge	V59 (SR?)	2
NGC 5286	13 ^h 46 ^m 26.58	-51°22'10".29	142141	17.1	19.3	yes			filled H α absorption	(SSG)	
NGC 5286	13 ^h 46 ^m 27.01	-51°22'29".94	71539	3.2	13.1	yes	yes		variable H α , H β emission	V74 (L)	2
NGC 5286	13 ^h 46 ^m 27.08	-51°22'30".68	70971	4.2	19.8	yes			noisy, filled H α absorption		
NGC 5286	13 ^h 46 ^m 27.73	-51°22'17".34	137375	13.2	18.6	yes	?		variable filled H α absorption	(RS)	
NGC 5286	13 ^h 46 ^m 28.99	-51°22'51".69	63415	31.9	13.1	yes	yes		variable H α emission	V60 (SR?)	2
NGC 5286	13 ^h 46 ^m 30.24	-51°22'7".37	127924	37.8	13.5	yes			H α emission, but close to detector edge		
NGC 5904	15 ^h 18 ^m 27.42	2°3'24".67	24106	122.9	14.5	yes		0.15	variable, filled H α absorption	V83 (RRLyr)	2
NGC 5904	15 ^h 18 ^m 32.15	2°5'2".00	82524	19.0	16.1	yes	yes		variable, filled H α absorption		
NGC 5904	15 ^h 18 ^m 32.85	2°5'41".49	80224	50.1	15.2	yes			variable, filled H α absorption		
NGC 5904	15 ^h 18 ^m 33.74	2°4'6".55	41637	45.8	21.2	yes	yes		noisy filled H α absorption	V5 (RRLyr)	2
NGC 5904	15 ^h 18 ^m 34.29	2°5'1".79	73350	19.1	16.4	yes	yes	0.15	variable, filled H α absorption		
NGC 5904	15 ^h 18 ^m 36.12	2°4'14".19	34416	57.4	19.3	yes			variable H α emission	(BSS)	
NGC 5904	15 ^h 18 ^m 36.14	2°4'16".30	34419	56.4	11.8	yes			variable H α emission	V84 (RV Tau)	2
NGC 6093	16 ^h 17 ^m 1.60	-22°58'29".20	96954	12.1	19.6	yes		0.22	H α emission	CX3 (CV)	8
NGC 6093	16 ^h 17 ^m 2.18	-22°58'46".10	47840	12.6	18.6	no			noisy, variable, filled H α absorption		
NGC 6093	16 ^h 17 ^m 2.56	-22°58'46".31	45658	12.6	17.5	yes	yes	0.21	variable, filled H α absorption		
NGC 6093	16 ^h 17 ^m 2.82	-22°58'33".88	44184	5.7	17.3	yes	?	0.18	variable H α emission		
NGC 6121	16 ^h 23 ^m 31.46	-26°30'57".83	9918	61.2	16.6	?		0.19	H α emission	CX12 (?)	8
NGC 6121	16 ^h 23 ^m 32.40	-26°30'45".47	9674	60.5	17.4	?			T Sco (CV)		9
NGC 6121	16 ^h 23 ^m 35.04	-26°31'19".03	8911	13.9	16.1	yes		0.15	filled H α absorption	107/N33 (EC)	2
NGC 6121	16 ^h 23 ^m 35.07	-26°32'4".03	4921	31.4	17.4	?		0.19	filled H α absorption	108/N36 (?)	2
NGC 6218	16 ^h 47 ^m 10.59	-1°56'40".04	24182	55.8	20.3	yes	?	0.21	filled H α absorption	CX10 (AB)	10
NGC 6218	16 ^h 47 ^m 12.31	-1°57'18".13	13339	36.5	19.6	yes			filled H α absorption	98/N11 (EC)	2
NGC 6218	16 ^h 47 ^m 12.42	-1°57'8".41	13226	29.7	19.4	?	yes		H α emission		
NGC 6218	16 ^h 47 ^m 13.57	-1°57'26".47	12224	33.1	19.4	?	yes		filled H α absorption		
NGC 6218	16 ^h 47 ^m 15.71	-1°56'46".78	19958	24.4	20.8	?		0.04	broad H α and H β emission	CX1 (CV)	11
NGC 6218	16 ^h 47 ^m 16.50	-1°57'23".75	9466	45.3	20.9	yes			variable H α , H β emission		
NGC 6218	16 ^h 47 ^m 16.65	-1°56'56".24	9431	37.1	18.7	?	yes		variable, filled H α absorption		
NGC 6266	17 ^h 1 ^m 1.68	-30°6'41".92	4201	16.2	18.9	yes	yes		variable H α emission		
NGC 6266	17 ^h 1 ^m 12.95	-30°6'44".59	708	10.8	15.5	yes	no		variable, filled H α absorption	V182 (RRLyr)	2
NGC 6266	17 ^h 1 ^m 12.16	-30°7'2".63	392	15.6	16.3	yes	?		variable, filled H α absorption	V156 (RRLyr)	2
NGC 6266	17 ^h 1 ^m 12.54	-30°6'22".03	3208	27.6	18.4	yes			very strong H α , H β emission, misclassified?	V13 (RRLyr)	2
NGC 6266	17 ^h 1 ^m 12.77	-30°6'45".05	5	4.3	12.8	yes	yes		very strong H α , H β emission, misclassified?	V190? (RRLyr)	2
NGC 6266	17 ^h 1 ^m 12.83	-30°6'46".78	2106	2.7	17.5	yes	?		variable, filled H α absorption	V188 (RRLyr)	2
NGC 6266	17 ^h 1 ^m 12.86	-30°6'54".94	6	5.6	14.0	yes	yes		variable, filled H α absorption, bad model?	V146 (CpII)	2
NGC 6266	17 ^h 1 ^m 12.94	-30°7'21".44	842	32.1	16.5	yes	?		variable, filled H α absorption	V139 (RRLyr)	2
NGC 6266	17 ^h 1 ^m 12.98	-30°6'19".30	63	30.2	14.9	no			variable H α , H β emission	V239 (L)	2
NGC 6266	17 ^h 1 ^m 13.18	-30°6'50".28	1772	5.1	17.8	yes	yes		variable H α emission	M62-VLA1 (BH)	12
NGC 6266	17 ^h 1 ^m 13.41	-30°5'59".07	12285	51.0	19.4	no	yes		H α emission		
NGC 6266	17 ^h 1 ^m 13.55	-30°6'57".45	222	12.7	15.9	yes			variable, filled H α absorption	V163 (RRLyr)	2
NGC 6266	17 ^h 1 ^m 13.81	-30°7'9".05	19	23.6	13.3	yes	?		variable H α emission		

Table A.2. cont.

Cluster	RA	Dec	ACS ID	d_c [']	V [mag]	mem.?	vrad?	d_X [']	Comment	Ident.	Ref.
NGC 6293	17 ^h 10 ^m 9 ^s 85	-26°34'57.61	152	5.1	16.0	yes			variable, filled H α absorption		
NGC 6388	17 ^h 36 ^m 14.48	-44°43'20.75	250190	55.4	15.8	yes	yes		variable H α , H β emission	V18 (W Vir)	2
NGC 6388	17 ^h 36 ^m 15.41	-44°44'14.90	133353	20.6	14.8	yes	?		variable H α , H β emission	V95 (SR)	2
NGC 6388	17 ^h 36 ^m 16.08	-44°44'9.51	128054	12.3	14.6	yes	no		variable H α , H β emission	V88 (SR)	2
NGC 6388	17 ^h 36 ^m 16.62	-44°44'0.71	233113	9.6	17.0	yes	yes		H α emission in single spectrum		
NGC 6388	17 ^h 36 ^m 17.09	-44°44'0.53	229862	7.4	15.3	yes	?		variable H α , H β emission	V98 (L)	2
NGC 6388	17 ^h 36 ^m 17.20	-44°44'14.85	119418	7.1	13.6	yes	yes		variable H α , H β emission	V73 (W Vir)	2
NGC 6388	17 ^h 36 ^m 17.29	-44°44'18.76	119389	11.0	12.8	yes			variable, filled H α absorption	V80 (RV Tau)	2
NGC 6388	17 ^h 36 ^m 17.47	-44°44'17.50	118083	10.1	16.6	yes			H α , H β emission	V69 (W Vir)	2
NGC 6388	17 ^h 36 ^m 17.60	-44°44'16.12	117361	9.2	15.3	yes	?		variable H α , H β emission	V72 (W Vir)	2
NGC 6388	17 ^h 36 ^m 18.42	-44°44'19.39	111469	17.2	13.6	yes	?		variable H α , H β emission	V2 (Mira Ceti)	2
NGC 6441	17 ^h 50 ^m 11.14	-37°3'53.05	1000228	53.1	15.0	?			variable H α , H β emission	V9 (L)	2
NGC 6441	17 ^h 50 ^m 12.18	-37°3'12.45	135507	12.7	14.2	yes	yes		variable H α , H β emission	V127 (W Vir)	2
NGC 6441	17 ^h 50 ^m 12.42	-37°2'52.62	260896	14.7	16.0	?			H α , H β emission, contaminated?		
NGC 6441	17 ^h 50 ^m 12.64	-37°3'12.13	131318	8.5	15.1	?			variable H α emission	V126 (W Vir)	2
NGC 6441	17 ^h 50 ^m 12.72	-37°2'38.05	258272	27.4	19.0	?			spectral changes, H α , H β and Ca II triplet emission	V135 (L)	2
NGC 6441	17 ^h 50 ^m 13.69	-37°3'16.36	121826	13.5	18.7	?			H α , H β emission, contaminated?	V139? (SR)	2
NGC 6441	17 ^h 50 ^m 15.63	-37°3'7.60	104171	30.9	15.3	?	?		variable H α , H β emission		
NGC 6441	17 ^h 50 ^m 15.76	-37°2'16.45	231739	58.5	14.0	?	?		variable H α , H β emission	V6 (W Vir)	2
NGC 6441	17 ^h 50 ^m 16.29	-37°2'40.65	227201	45.9	16.6	?			variable H α , H β emission	V2 (Mira Ceti)	2
NGC 6441	17 ^h 50 ^m 17.23	-37°3'50.01	91313	67.1	16.4	yes			variable H α , H β emission	V1 (Mira Ceti)	2
NGC 6522	18 ^h 3'32.50	-30°2'3.02	80	19.7	13.2	yes			variable, filled H α absorption		
NGC 6522	18 ^h 3'35.42	-30°2'6.47	88	18.7	14.3	yes	?		variable H α emission		
NGC 6541	18 ^h 8'0.99	-43°43'9.53	44127	21.7	18.5	no	yes	0.05	variable, filled H α absorption	(SSG)	
NGC 6541	18 ^h 8'2.22	-43°42'58.15	40733	4.8	17.4	yes	yes	0.18	broad H α emission	(RS)	
NGC 6541	18 ^h 8'3.60	-43°43'4.50	36939	17.3	17.9	yes	no	0.10	variable, filled H α absorption	(SSG)	
NGC 6656	18 ^h 36 ^m 21.68	-23°53'35.07	68961	52.2	15.7	yes	yes	0.29	variable, filled H α absorption	Source 33? (RS Cvn?)	13
NGC 6656	18 ^h 36 ^m 21.78	-23°54'13.36	68665	29.8	13.4	yes	yes		variable H α absorption	V24 (W Vir)	2
NGC 6656	18 ^h 36 ^m 23.79	-23°54'18.38	37810	2.3	13.7	yes	?		variable, filled H α absorption		
NGC 6656	18 ^h 36 ^m 24.05	-23°54'29.60	37211	12.6	10.7	yes	no		variable filled H α absorption	V35 (SR)	2
NGC 6656	18 ^h 36 ^m 24.10	-23°54'33.27	36997	16.3	18.2	yes	?		filled H α absorption		
NGC 6656	18 ^h 36 ^m 24.20	-23°54'10.32	63613	7.7	20.0	?	yes	0.49	noisy, broad H α emission, multiple spectral components?		
NGC 6656	18 ^h 36 ^m 24.69	-23°54'35.69	35776	21.3	18.9	yes			broad H α , H β , He emission	CV1 (CV)	2
NGC 6681	18 ^h 43 ^m 10.38	-32°17'3.09	39915	41.4	20.6	no	?		variable H α , H β emission		
NGC 6681	18 ^h 43 ^m 10.78	-32°17'54.57	21588	34.0	13.7	yes	no		variable, filled H α absorption	(CV)	
NGC 6681	18 ^h 43 ^m 11.78	-32°17'55.22	19706	26.6	22.7	yes		0.17	broad H α , H β and He emission	CX19 (AB?)	14, 15
NGC 6752	19 ^h 10 ^m 55.55	-59°59'17.40	14153	29.0	17.7	yes		0.49	filled H α absorption	CX2 (CV)	14
NGC 6752	19 ^h 10 ^m 56.00	-59°59'37.37	13797	44.0	19.6	yes		0.12	broad H α , H β and He emission		
NGC 7078	21 ^h 29 ^m 56.58	12°10'40.19	186117	46.7	14.6	yes	?		filled H α absorption		
NGC 7078	21 ^h 29 ^m 57.83	12°10'0.50	176122	7.3	16.0	yes	yes		variable H α absorption	V131 (RRLyr)	2
NGC 7078	21 ^h 29 ^m 57.84	12°9'51.99	95810	11.6	15.9	yes	yes		variable, filled H α absorption	V130 (RRLyr)	2
NGC 7078	21 ^h 29 ^m 58.31	12°10'2.80	172701	1.6	15.5	yes		0.13	P Cygni of H, He	V125 (LMXB)	2
NGC 7078	21 ^h 29 ^m 59.15	12°10'7.20	165986	13.5	13.6	yes			variable H α , H β emission	V86 (W Vir)	2
NGC 7078	21 ^h 29 ^m 59.43	12°10'21.89	164189	26.3	19.1	yes			variable H α emission		
NGC 7078	21 ^h 29 ^m 59.47	12°9'43.80	83983	24.2	14.8	yes	yes		variable H α emission		
NGC 7078	21 ^h 30 ^m 0.62	12°10'1.35	154446	33.6	13.0	yes	?		emission from H α wings		
NGC 7089	21 ^h 33 ^m 23.64	0°48'59.89	179324	56.0	14.5	yes	?		variable, filled H α absorption		
NGC 7089	21 ^h 33 ^m 23.84	0°49'12.91	178318	48.8	12.7	yes	?		variable H α , H β emission	V5 (W Vir)	2

Table A.2. cont.

Cluster	RA	Dec	ACS ID	d_c ["]	V [mag]	mem.?	rad?	d_x ["]	Comment	Ident.	Ref.
NGC 7089	21 ^h 33 ^m 23.98s	0°49'12".48	177434	46.9	19.8	yes			variable H α emission		
NGC 7089	21 ^h 33 ^m 24.34s	0°49'9".46	175600	42.6	16.3	yes	?		variable, filled H α absorption		
NGC 7089	21 ^h 33 ^m 24.93s	0°48'43".37	171867	51.1	16.2	yes	yes		variable, filled H α absorption	V51 (RRLyr)	2
NGC 7089	21 ^h 33 ^m 25.09s	0°48'49".44	170746	44.8	13.1	yes	no		weak emission from H α wings		
NGC 7089	21 ^h 33 ^m 25.86s	0°49'4".93	165509	25.6	18.4	yes	yes		variable, filled H α absorption		
NGC 7089	21 ^h 33 ^m 26.79s	0°48'33".64	219411	50.2	16.0	yes	yes		variable, filled H α absorption	V22 (RRLyr)	2
NGC 7089	21 ^h 33 ^m 27.52s	0°49'59".64	81620	36.7	13.3	yes	yes		variable H α , H β emission	V6 (W Vir)	2
NGC 7089	21 ^h 33 ^m 27.88s	0°49'53".45	79550	32.5	12.7	yes	?		emission from H α wings		
NGC 7099	21 ^h 40 ^m 20.96s	-23°10'43".27	51191	16.5	18.0	yes	yes		variable H α absorption	(SSG)	
NGC 7099	21 ^h 40 ^m 21.80s	-23°10'50".55	26939	5.4	14.8	yes	yes		variable, filled H α absorption	V15 (RRLyr)	2
NGC 7099	21 ^h 40 ^m 21.80s	-23°10'9".11	49462	38.6	11.7	yes	?		emission from H α wings		
NGC 7099	21 ^h 40 ^m 22.22s	-23°10'47".46	25532	1.4	16.1	yes	yes	0.28	variable H α emission, between RGB and HB	A2 (?)	16
NGC 7099	21 ^h 40 ^m 22.95s	-23°10'49".60	23423	11.7	20.3	yes	yes	0.12	broad H α and H β emission	(CV)	

Notes. ^(a) F625W. AB: chromospherically active binary, BL Her: BL Herculis pulsating variable, CplI: Type II Cepheid pulsating variable, CV: cataclysmic variable, EA: eclipsing semi-detached binary (Algol-type), EC: eclipsing contact binary, EW: eclipsing low mass contact binary, L: slow irregular variable, LMXB: low-mass X-ray binary, LPV: long-period variable, MSP: millisecond pulsar, SR: semiregular variable, SSG: sub-subgiant, RS: red straggler, RS Cvn: close eruptive binary (RS Canum Venaticorum), W Vir: W Virginis pulsating variable

References. (1) Heinke et al. (2005); (2) Clement et al. (2001); (3) Albrow et al. (2001); (4) Kunder et al. (2013); (5) Kaluzny et al. (2016); (6) Lebzelter & Wood (2016); (7) Cool et al. (2013); (8) Heinke et al. (2003); (9) Dieball et al. (2010); (10) Bassa et al. (2004); (11) Lu et al. (2009b); (12) Chomiuk et al. (2013); (13) Webb et al. (2004); (14) Pooley et al. (2002); (15) Lugger et al. (2017); (16) Lugger et al. (2007).